March 1992 • NREL/TP-411-4752

Novel Thin-Film $CuInSe_2$ Fabrication

Annual Subcontract Report
1 March 1990 - 30 April 1991

G.D. Mooney
A.M. Hermann
University of Colorado
Boulder, Colorado

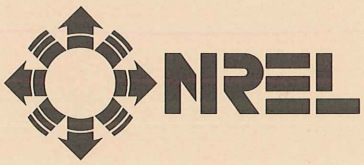

National Renewable Energy Laboratory
A Division of Midwest Research Institute
Operated for the U.S. Department of Energy
Under Contract No. DE-AC02-83CH10093

NREL/TP-411-4752 • UC Category: 273 • DE92001222

NREL/TP--411-4752

DE92 001222

Novel Thin-Film $CuInSe_2$ Fabrication

Annual Subcontract Report 1 March 1990 - 30 April 1991

G.D. Mooney
A.M. Hermann
University of Colorado
Boulder, Colorado

NREL technical monitor: R. Mitchell

National Renewable Energy Laboratory
(formerly the Solar Energy Research Institute)
1617 Cole Boulevard
Golden, Colorado 80401-3393
A Division of Midwest Research Institute
Operated for the U.S. Department of Energy
under Contract No. DE-AC02-83CH10093

Prepared under Subcontract No. XC-0-10012-1

March 1992

MASTER

DISTRIBUTION OF THIS DOCUMENT IS UNLIMITED

On September 16, 1991 the Solar Energy Institute was designated a national laboratory, and its name was changed to the National Renewable Energy Laboratory.

NOTICE

This report was prepared as an account of work sponsored by an agency of the United States government. Neither the United States government nor any agency thereof, nor any of their employees, makes any warranty, express or implied, or assumes any legal liability or responsibility for the accuracy, completeness, or usefulness of any information, apparatus, product, or process disclosed, or represents that its use would not infringe privately owned rights. Reference herein to any specific commercial product, process, or service by trade name, trademark, manufacturer, or otherwise does not necessarily constitute or imply its endorsement, recommendation, or favoring by the United States government or any agency thereof. The views and opinions of authors expressed herein do not necessarily state or reflect those of the United States government or any agency thereof.

Printed in the United States of America
Available from:
National Technical Information Service
U.S. Department of Commerce
5285 Port Royal Road
Springfield, VA 22161

Price: Microfiche A01
Printed Copy A04

Codes are used for pricing all publications. The code is determined by the number of pages in the publication. Information pertaining to the pricing codes can be found in the current issue of the following publications which are generally available in most libraries: *Energy Research Abstracts (ERA)*; *Government Reports Announcements* and Index (*GRA* and I); *Scientific and Technical Abstract Reports (STAR)*; and publication NTIS-PR-360 available from NTIS at the above address.

DISCLAIMER

Portions of this document may be illegible electronic image products. Images are produced from the best available original document.

Preface

This report has been excerpted from the Ph.D. dissertation of G. David Mooney, submitted to the University of Arkansas and accepted in December 1990, and is based on work performed at the Solar Energy Research Institute.

Table of Contents

	Introduction	1
1.0	Experimental Considerations and Design	3
1.1	Study of Precursor Films	5
2.0	The Formation of Thin Film $CuInSe_2$ by Rapid Thermal Processing	12
2.1	Rapid Thermal Processing of Elemental Sandwich Structures	14
2.2	Rapid Thermal Processing of Co-Deposited Cu, In, and Se Thin Films	20
2.2 i	Composition Studies of Co-Deposited CIS Thin Films Formed by RTP	23
2.2 ii	X-Ray Diffraction Studies of Co-Deposited CIS Thin Films Formed by RTP	29
2.2 iii	Optical Studies of Co-Deposited CIS Thin Films Formed by RTP	33
2.2 iii (a)	General Theory of the Optical Properties of Semiconductors	34
2.2 iii (b)	Experimental Determination of the Optical Properties of CIS	36
2.2 iv	Scanning Electron Microscopy of CIS Thin Films Formed by RTP	45
2.2 v	Large Single Crystal CIS Formation by Rapid Thermal Processing of Unreacted Co-Deposited Thin Films	48
3.0	CIS/CdS Device Fabrication Using CIS Formed by Rapid Thermal Processing	51
4.0	References	55
5.0	Abstract	57

List of Figures

Figure 1 Scanning Electron Micrographs of Al_2O_3/Mo/Cu/In at Ts = 170 and 25°C, Al_2O_3/Mo/In/Cu at Ts = 170°C, and Al_2O_3/Mo/Cu + In at Ts =170°C 7

Figure 2 Scanning Electron Micrographs of Glass/Cu at Ts = 25°C and Glass/In at Ts = 25°C 8

Figure 3 Auger Depth Profile of Al_2O_3/Mo/Cu/In Structure 9

Figure 4 Auger Depth Profile of Al_2O_3/Mo/In/Cu Structure 10

Figure 5 XRD Pattern of Al_2O_3/Mo/Cu/In Structure Deposited at a Substrate Temperature of 170°C 11

Figure 6 XRD Pattern of Al_2O_3/Mo/Cu + In Structure Deposited at a Substrate Temperature of 170°C 11

Figure 7 Schematic AET ADDAX® Rapid Thermal Processor 12

Figure 8 Sample Annealing Profile Generated by RTP Control Computer 13

Figure 9 Initial Layered Structure Annealed by RTP 14

Figure 10 XRD Data of a Layered Sample Annealed at 600°C For 15 Seconds 16

Figure 11 Scanning Electron Micrographs of Surface and Edge of Above Layered Sample 16

Figure 12 Scanning Electron Micrograph of a Al_2O_3/Cu/In/Se/In/Cu Sample Deposited at Ts = 170°C as a Precursor and After Processing at 600°C 17

Figure 13 Layered Sample Annealed at 600°C for 15 Seconds 18

Figure 14 Scanning Electron Micrograph of a Al_2O_3/Cu/In (3x) as a Precursor Deposited at Ts = 170°C and After Annealing at 600°C 19

Figure 15 Schematic of Vacuum System Used in the Co-Deposition of CIS Thin Film Precursors 21

Figure 16 Structure of Vacuum Co-Deposited Precursors....22

Figure 17 RTP Experimental Matrix Showing Parameters Varied and Their Ranges....23

Figure 18 The Change in Δx for Stoichiometric Samples....24

Figure 19 The Change in Δz for Stoichiometric Samples....25

Figure 20 The Change in Δx for Cu-Poor Samples....25

Figure 21 The Change in Δz for Cu-Poor Samples....26

Figure 22 The Change in Δx for Cu-Rich Samples....26

Figure 23 The Change in Δz for Cu-Rich Samples....27

Figure 24 The Change in Δx Versus the Starting Atomic Percent Cu For Samples Processed in all Three Composition Regions....27

Figure 25 The Change in Δz Versus the Starting Atomic Percent Se For Samples Processed in all Three Composition Regions....28

Figure 26 XRD Data of a Stoichiometric Co-Deposited Sample Annealed Under Conditions Given in Figure 16....30

Figure 27 XRD Data Comparing (112) Peak Intensities of the Film Shown in Figure 24 and its Precursor....30

Figure 28 Integrated (112) Peak Intensities for Films Processed At Conditions Shown....31

Figure 29 XRD Data of a Cu-Poor Sample Processed at Corner 6 Of the Experimental Matrix....32

Figure 30 XRD Data of a Cu-Rich Sample Processed at Corner 6 Of the Experimental Matrix....32

Figure 31 Reflection and Transmission Model for Air/CIS/Glass/Air System....37

Figure 32 Plot of Log of α Versus Incident Photon Energy for a Co-Deposited, Stoichiometric Sample Processed Under The Conditions of Corner 8 and its Precursor....39

Figure 33 Plot of Log of α Versus Incident Photon Energy for a Co-Deposited, Cu-Poor Sample Processed Under The Conditions of Corner 8 and its Precursor....39

Figure 34 Plot of Log of α Versus Incident Photon Energy for a Co-Deposited, Cu-Rich Sample Processed Under The Conditions of Corner 8 and its Precursor....40

Figure 35 Plot of Log of α Versus Incident Photon Energy for a Co-Deposited, Stoichiometric Sample Processed Under Conditions Indicated and Their Precursors....41

Figure 36 Plot α^2 Versus Incident Photon Energy for a Co-Deposited, Stoichiometric Sample Processed Under The Conditions of Corner 8....42

Figure 37 Plot of α^2 Versus Incident Photon Energy for a Co-Deposited, Cu-Poor Sample Processed Under The Conditions of Corner 8....43

Figure 38 Plot of α^2 Versus Incident Photon Energy for a Co-Deposited, Cu-Rich Sample Processed Under The Conditions of Corner 8....43

Figure 39 Plot of α^2 Versus Incident Photon Energy Comparing The Transitions of Cu-Poor and Cu-Rich Films....44

Figure 40 Scanning Electron Micrographs of Stoichiometric Precursor and Film Processed Under the Conditions Of Corner 6 (CIS and Mo)....46

Figure 41 Scanning Electron Micrographs of a Cu-Poor Film Processed Under the Conditions Of Corner 7....47

Figure 42 Scanning Electron Micrographs of a Cu-Rich Film Processed Under the Conditions Of Corner 8....47

Figure 43 Scanning Electron Micrographs of Large Grain CIS (Multiple Views)....49

Figure 44 XRD Data of Sample with 20μm Single Crystals....50

Figure 45 (112) Peaks Comparison of Sample Shown in Figure 26 and the Sample with 20μm Single Crystals....50

Figure 46 Tri-Layer Device Structure.....52

Figure 47 CIS Device Results for Structure Shown in Figure 44.....53

List of Tables

Table I	Variable Parameters and their Ranges for the RTP Experiment	3
Table II	Matrix of Films Grown for Morphology and Microstructure Studies of Metallic Precursors	5
Table III	Variables Held Constant in the RTP of Co-Deposited Cu, In, and Se Thin Films	20
Table IV	Comparison of Precursor and Annealed Sample Composition	24
Table V	Values for A* and Subsequent Hole Effective Masses	45

Introduction

One of the major drawbacks for the commercial fabrication of $CuInSe_2$ by one of the leading methods – selenization of Cu/In layers with H_2Se – is the use of H_2Se, which is highly toxic. There are several interesting possibilities that would allow formation of $CuInSe_2$ without the use of H_2Se. Among these is Rapid Thermal Processing (RTP) of elemental sandwiched layers of Cu, In, and Se, or of co-evaporated Cu/In/Se films. To perform proof-of-concept work along these lines is the approach of this research.

RTP is a well-established method of rapidly achieving temperatures necessary to melt and recrystallize materials such as Si and silicides. RTPs can rapidly and uniformly heat large surface areas to hundreds of degrees Celsius.

The most promising method of rapid recrystallization of ternary semiconductors we have studied to date is the rapid thermal processing of unreacted thin films. This method uses tungsten quartz lamps to heat the sample by radiation and offers several advantages over more conventional processes. The RTP is readily scalable from the research to the production level, the processing time is very conducive to mass production, and the process is executed in an inert atmosphere. The desire to explore processes that have these characteristics was the stimulus of this work.

The approach to the experiment was a complicated one because of the extremely large number of variables involved. When considering the design of the first phase of the experiment, we essentially divided it into two sections: 1) fabrication of the precursor film and 2) processing of the precursor film. The objective of the first phase of the work was to fabricate the thin films by RTP, then fully characterize them, to demonstrate the viability of the process as a method by which to make device-quality CIS.

The second phase, and the ultimate goal, was to demonstrate that material made by this method could be used to make an active photovoltaic device. As will be discussed in the remainder of this report, we have successfully obtained both of these objectives.

1.0 Experimental Considerations and Design

Since no previous work had been done by RTP in the fabrication of ternary semiconducting thin films, the lack of a data base to draw upon and the large number of variables necessitated a careful approach to the design of the experiment. As mentioned above, the first phase of the experiment involved demonstrating the ability of the process to produce CIS with characteristics comparable to those of material fabricated by more conventional methods. We began by considering the two distinct portions of the experiment. Specifically, we needed to determine which type of precursor film we were going to process, and how we were going to process it. Table I lists the variable parameters of each portion, and the choices and/or ranges of each.

Table I. ***Variable Parameters and their Ranges for the RTP Experiment.***

Precursor Variables	
Variable	Choices/Ranges
Type of Substrate	Polycrystalline or Monocrystalline
Material of Polycrystalline Substrate	Alumina or Glass
Method of Deposition	Co-Deposition of the Elements or Elemental Layered Structures
Co-Deposition	
•Atomic Flux Rates	0.1 – 20 Å/s
•Film Thickness	500 Å – 4 μm
•Substrate Temperature	25 °C – 500 °C
•Composition of Film	(To be discussed)

Table I, Continued

Precursor Variables

Variable	Choices/Ranges
Elemental Layers	
•Ordering of Layers	Cu/In/Se or In/Se/Cu etc.
•Number of "Sandwiches"	1 – 10 (or more)
•Thickness of Individual Layers	100 Å – 2 μm
•Composition	– –
•Substrate Temperature	25 – 500 °C

Processing Variables

Variable	Choices/Ranges
Temperature Ramp-Up Rate	1 – 250 °C/s
Final Anneal Temperature	25 – 1200 °C
Final Anneal Time	0 – ∞ seconds
Intermediate Steps	
•Number	0 – ∞
•Ramp Rate	1 – 250 °C/s
•Intermediate Anneal Temperature	25 – 1200 °C
•Intermediate Anneal Time	0 – ∞ seconds
Temperature Ramp-Down Rate	Limited by Exponential Nature of Natural Cool-Down
Processing Atmosphere	Argon, Nitrogen, H_2Se, Air

The choice of many of the variables was determined by the results we wished to obtain. We would not choose to anneal for long periods of time, or to anneal in

an atmosphere of H_2Se, for example, because these choices would offer no advantage over more conventional methods. The design of the experiment, then, consisted of deciding which variables to hold constant and at which value to hold them, and which parameters to vary and over what ranges. To make the most intelligent choices possible, we conducted a set of preliminary experiments designed to help us determine which variables most affected the process, and what ranges yielded the most positive results.

1.1 Study of Precursor Films

To begin our study, we first chose to explore the morphology and microstructure of layered and co-deposited metal (Cu and In) films [1]. In this experiment, we varied the type of deposit, the order of the layers, the layer thicknesses, the substrate temperature, and the type of substrate material. The series of films grown is shown in Table II.

Table II. ***Matrix of Films Grown to Study the Morphology and Microstructure of Metallic Precursors. An X Indicates a Film has been Grown for Those Conditions.***

	Substrate Temperature	
Film Structure	25 °C	170 °C
Substrate/Mo/Cu+In	X	X
Substrate/Mo/Cu/In	X	X
Substrate/Mo/In/Cu	X	X
Substrate/Mo/Cu/In+Ga	X	X
Substrate/Mo/Ga/Ga+Cu/In		X

Table II Continued

	Substrate Temperature	
Film Structure	25 °C	170 °C
Substrate/Mo/Cu+Ga/In		X
Substrate/Mo/Cu/In+Ga		X
Glass/Mo/Cu	X	
Glass/Mo/In	X	

The notation "Substrate/Mo/Cu/In" indicates the film was deposited in layers; Mo was deposited directly onto the substrate, then a layer of Cu, then a layer of In. The notation "Cu+In" indicates that Cu and In were co-deposited. Each structure listed was duplicated on Corning 7059 glass and alumina (Al_2O_3) at thicknesses t (Cu=1000Å, In=2200Å) and 2t (Cu=2000Å, In=4400Å) for the layered samples and 3200 and 6400 Å for the co-deposited samples. The elevated substrate temperature was chosen to be just above the melting point of In (156 °C).

The results of this experiment showed a very strong dependence of the morphology and alloying on all of the variables explored. A comparison of the morphologies for copper and indium layers deposited at the different parameters indicated in Figure 1 shows some of the primary features observed in the precursor study. The differences in the films are dramatic and can readily be seen. The Al_2O_3/Mo/Cu/In and Al_2O_3/Mo/Cu+In films deposited at 170 °C appear to be the most dense with the smoothest morphologies. The Al_2O_3/Mo/Cu/In film deposited at 25 °C has consistent morphology across the substrate, but the materials have coalesced, leaving island formations and subsequent voids. Voids are extremely undesirable when considering device-

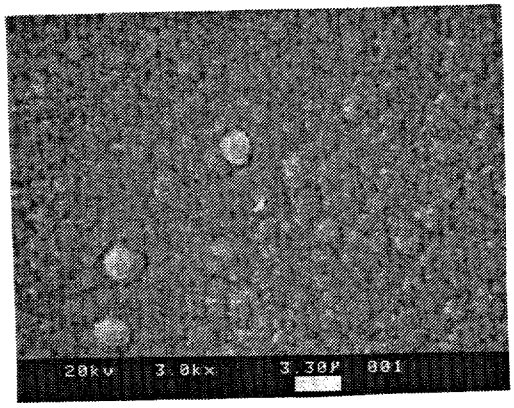

(a)

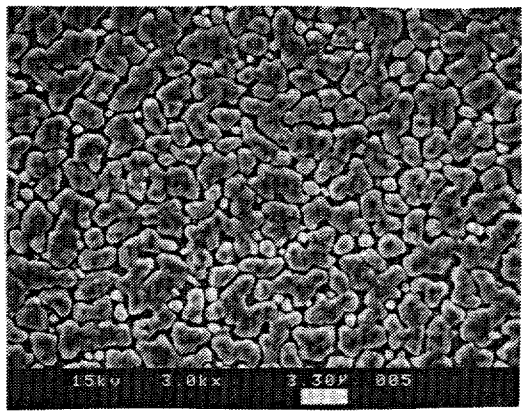

(b)

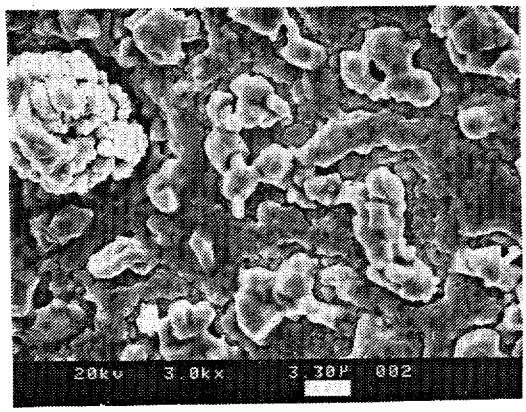

(c)

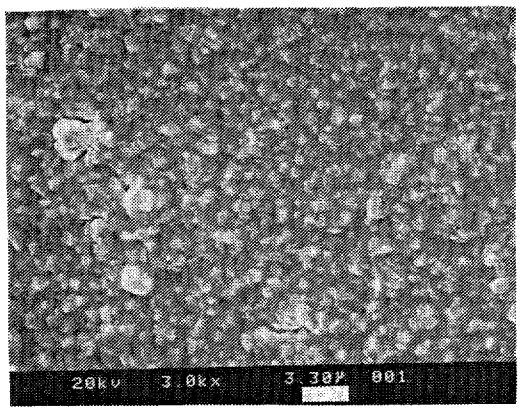

(d)

Figure 1. *Scanning Electron Micrographs of (a) Al_2O_3/Mo/Cu/In at Ts = 170 °C, (b) Al_2O_3/Mo/Cu/In at Ts = 25 °C, (c) Al_2O_3/Mo/In/Cu at Ts = 170 °C, and (d) Al_2O_3/Mo/Cu+In at Ts = 170 °C.*

quality material because of resulting electrical shorts between the window material and the back contact. The most interesting comparison is between Al_2O_3/Mo/Cu/In and the Al_2O_3/Mo/In/Cu films. Although the composition is identical, the difference in the morphology is pronounced, with the latter film

having a very non-uniform, large surface roughness. This is a consequence of this particular method of deposition. The temperature of evaporating Cu and In vapor in a 10^{-6} Torr vacuum is 857 °C and 597 °C respectively. Since the melting point of In (156 °C) is much lower than that of Cu (1083 °C), Cu atoms impinging on an In layer would cause localized melting of the In. The localized molten area much more readily alloyed with the Cu causing a very uneven and rough morphology. In the other case, In atoms impinging on a Cu layer did not produce localized melting of Cu. The alloying reactions were then solid-gas in nature and hence more uniform and stable. Figure 2 shows SEMs of an elemental Cu and an elemental In layer. These support the fact that the resulting alloy films were not a result of individual layer morphology. As is seen, the Cu

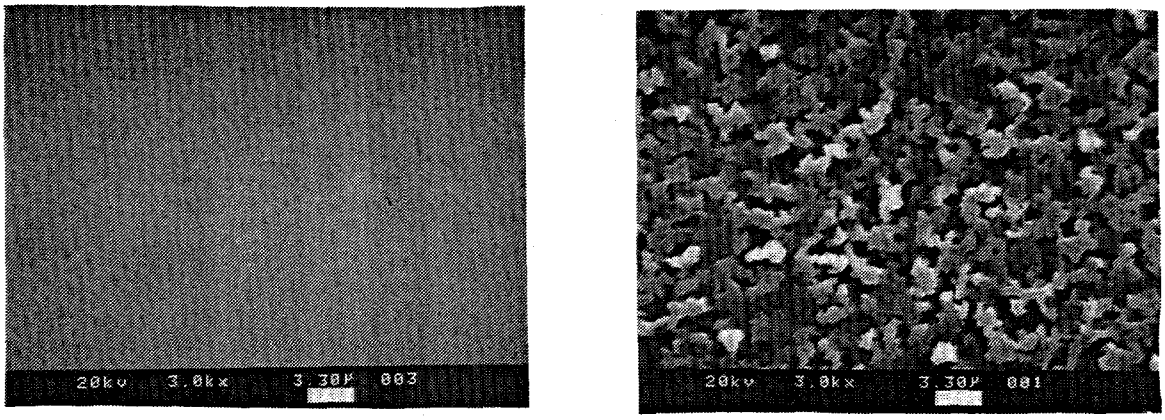

(a) (b)

Figure 2. ***Scanning Electron Micrographs of (a) Glass/Cu at Ts = 25°C, (b) Glass/In at Ts = 25 °C.***

film is completely smooth on the scale shown, while the In film is made of In crystallites about two microns in size that uniformly cover the substrate.

This scenario is supported by Auger analysis. Figure 3 shows the compositional depth profile of the Al_2O_3/Mo/Cu/In structure. With the exception of the surface of the film, which has a "spike" of In, the distribution of the elements is homogeneous throughout, indicating uniform alloying. Conversely, the depth profile of the Al_2O_3/Mo/In/Cu structure (Figure 4) shows the element distribution to be somewhat inhomogeneous. The Cu and In spikes perhaps correspond to areas like the nodule shown in Figure 1 (c).

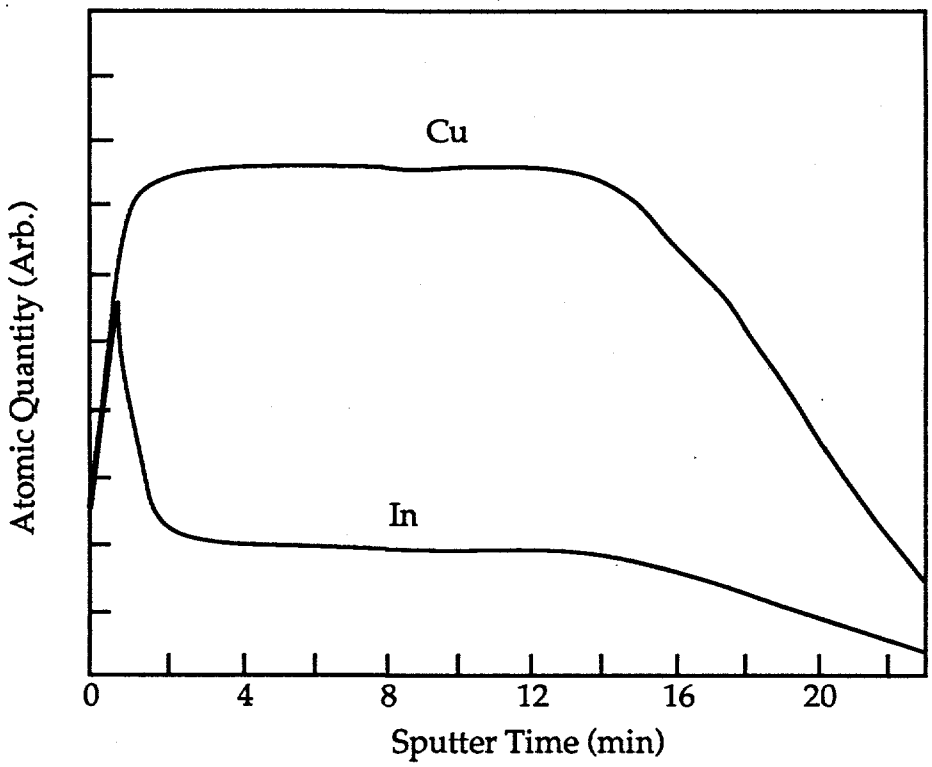

Figure 3. ***Auger Depth Profile of Al_2O_3/Mo/Cu/In Structure.***

The SEMs of all films from Table II not already shown may be found in Appendix A of Ref. 2.

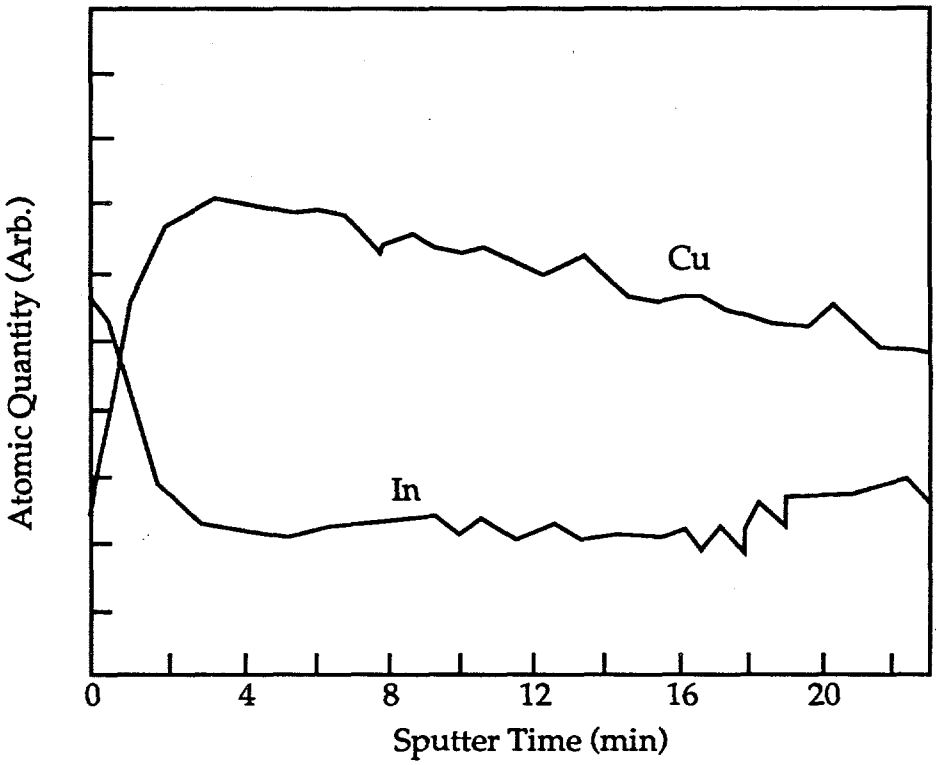

Figure 4. ***Auger Depth Profile of Al_2O_3/Mo/In/Cu Structure.***

The conclusion drawn from the preliminary precursor study was the Cu/In and Cu+In films deposited at temperatures above the melting point of In had morphologies most conducive for either selenization by selenium layers, H_2Se, or co-evaporation of selenium. For completeness, we then took XRD measurements of the Al_2O_3/Mo/In/Cu and Al_2O_3/Mo/Cu+In samples. These patterns are shown in Figures 5 and 6. The data show the formation of the alloy Cu_7In_4 with elemental In present. The presence of the crystallized elemental In is consistent with the Cu-In alloy formation because the atomic ratios in the depositions were 1:1. The formation of the Cu_7In_4, then, used all the available Cu, leaving excess In to crystallize.

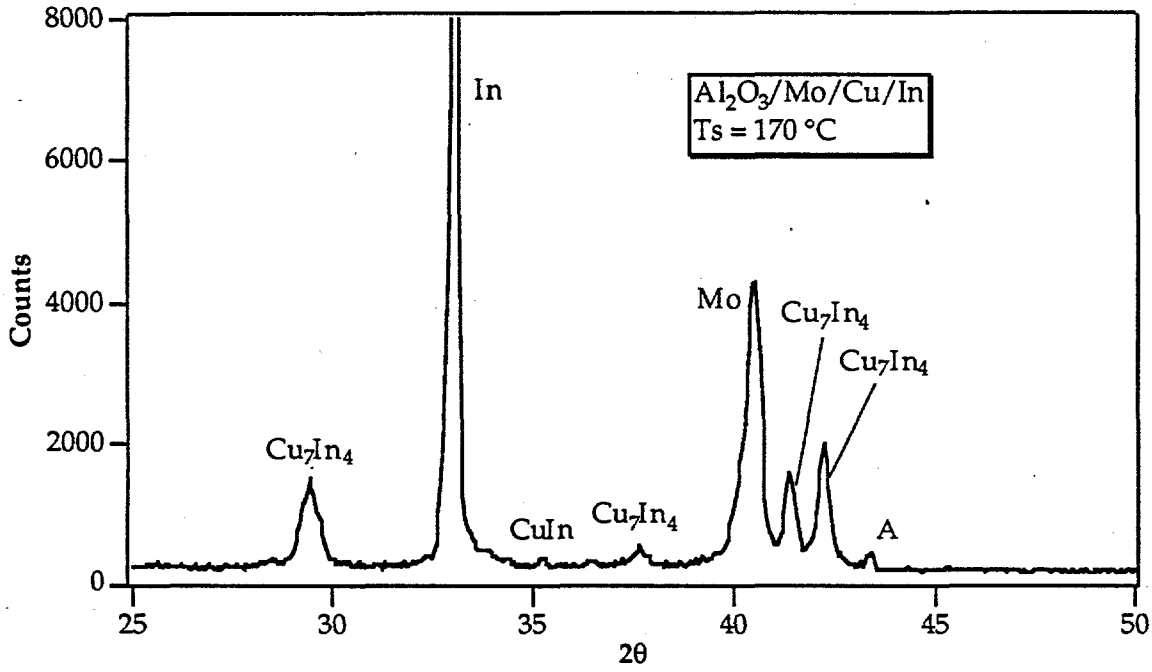

Figure 5. *XRD Pattern of Al_2O_3/Mo/Cu/In Structure Deposited at a Substrate Temperature of 170 °C.*

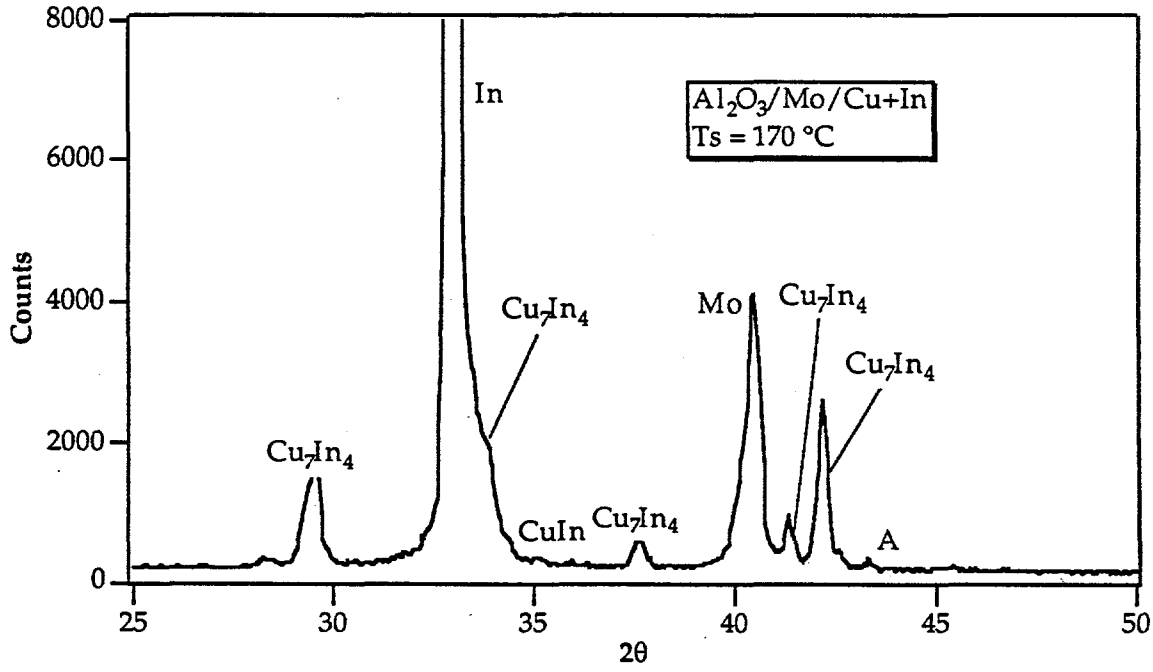

Figure 6. *XRD Pattern of Al_2O_3/Mo/Cu+In Structure Deposited at a Substrate Temperature of 170 °C.*

2.0 The Formation of Thin Film $CuInSe_2$ by Rapid Thermal Processing

Rapid thermal processing is a relatively new technology with growing uses in the semiconductor industry. The development stems from a need in the Si industry to anneal different materials in contact with one another without the interdiffusion associated with lengthy, conventional thermal anneal. Our efforts have been an attempt to extend the technology's usefulness to the fabrication of ternary semiconductor thin films by recrystallization of unreacted films.

To conduct our RTP experiments, we have used a commercially available, AET ADDAX®, computer- interfaced rapid thermal processor (RTP). A schematic of this system is shown in Figure 7. The RTP heats the sample by radiation using a bank of 18 halogen quartz lamps. With the computer, the

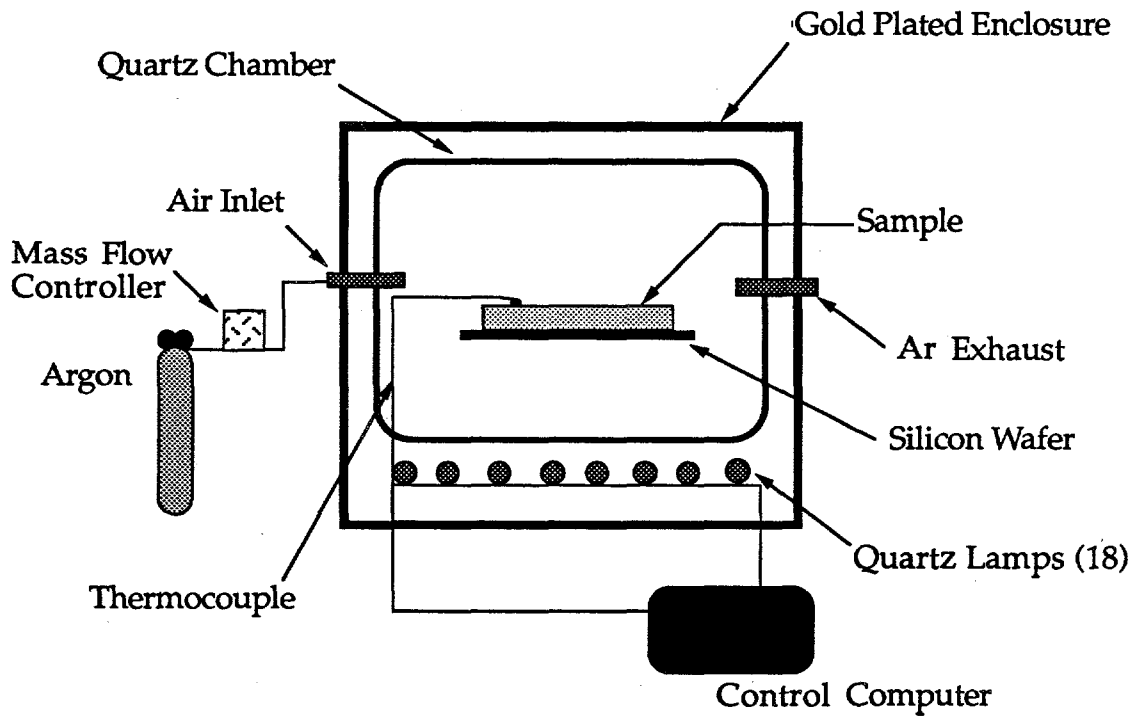

Figure 7. ***Schematic AET ADDAX® Rapid Thermal Processor.***

operator has control of the processing temperature, processing time, the rate of temperature increase, and the atmosphere in which the sample is annealed. The temperature is controlled by a thermocouple that is in direct thermal contact with the sample. The thermocouple controls the power output of the lamps via a closed loop with the computer software; this output is based on the desired temperature input by the operator. The sample is enclosed in a sealed quartz chamber where process gases are introduced using mass flow controllers. The lamps and quartz chamber are in turn enclosed in a gold-plated, aluminum cavity. A sample annealing "recipe" generated by the control computer is shown in Figure 8. This particular recipe has a temperature ramp rate of 10 °C/s, a final anneal time of 30 seconds, and a final anneal temperature of 700 °C. The cool down of the sample would be uncontrolled (natural). The thermocouple was calibrated regularly and was accurate to ± 2 °C during the anneals.

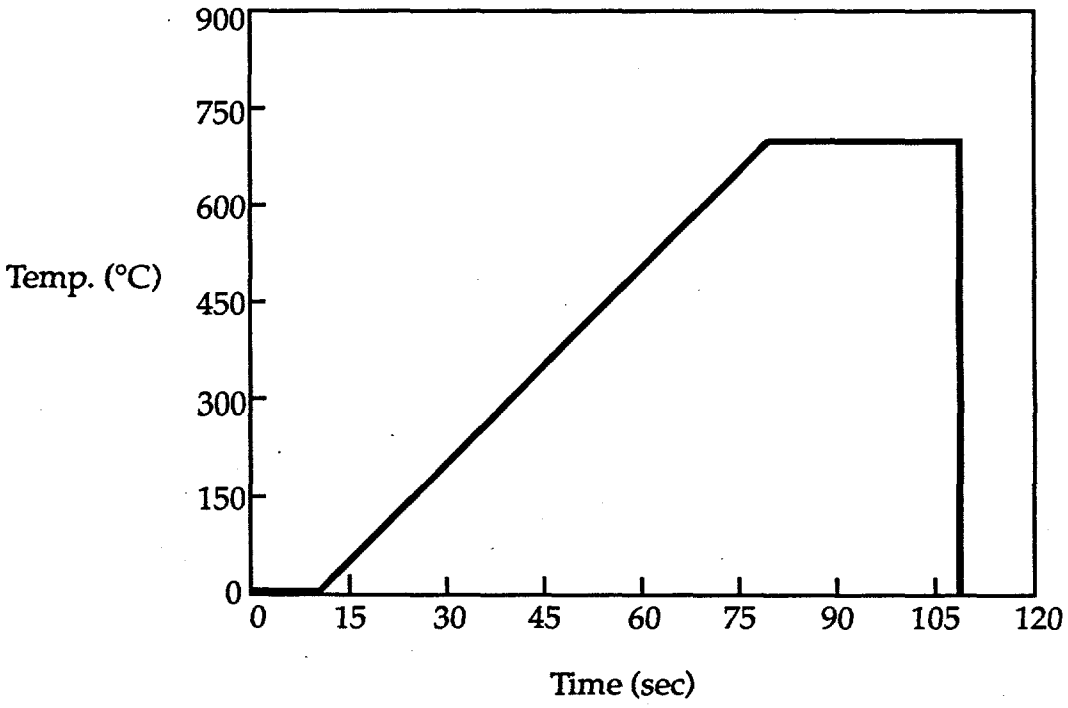

Figure 8. ***Sample Annealing Profile Generated by RTP Control Computer***

2.1 Rapid Thermal Processing of Elemental Sandwich Structures

To experiment with the RTP of vacuum deposited layered samples, films of the structure Al_2O_3/Mo/Cu/In/Se/In/Cu (Figure 9) were fabricated with the substrate held at room temperature.

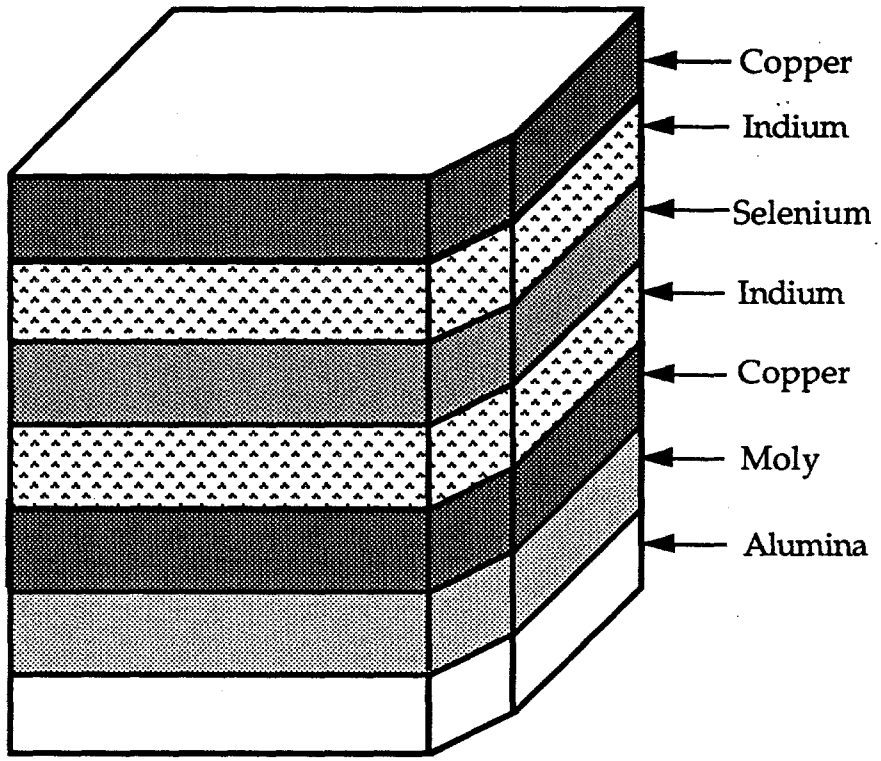

Figure 9. ***Initial Layered Structure Annealed by RTP.***

The ordering of the layers represented a compromise between obtaining good morphology with the Cu/In ordering and the desire to inhibit Cu-Se binary formation by separating the Cu and Se layers. In this structure, the layer thicknesses were targeted to yield a stoichiometric film. The thicknesses were

Al_2O_3/Mo/1000Å/2200Å/9200Å/2200Å/1000Å. A group of these films was processed at RTP conditions ranging from final anneal temperatures of 400-700 °C and anneal times from 10-30 seconds. Ramp-up rates were in the range of 35 °C/s. In all cases, the chamber was purged thoroughly with argon flowing at eight liters/min prior to the anneal. The samples were then annealed in a 0.1 liters/min flowing argon atmosphere and subsequently cooled naturally.

In all cases of films processed with this layer ordering and these layer thicknesses, the resulting annealed film experienced excessive Se loss. The composition was determined by Electron Probe for Microanalysis (EPMA). A typical post annealed composition was determined to be 30.43/30.97/38.60 where this notation stands for atomic percent Cu/atomic percent In/atomic percent Se and will be used often in the remainder of the discussion. (A stoichiometric film would be represented by 25.00/25.00/50.00.) The explanation for the Se evaporation stems from the thickness of the Se layer. Since Se is the most easily volatilized of the three elements, much of the Se evaporated before it had a chance to diffuse throughout the bulk of the film and react with the other elements.

Even though large amounts of Se evaporated, XRD analysis showed a majority of CIS formation (Figure 10). Also, as might be expected from the precursor study, the absence of adequate Se to form pure CIS allowed the formation of Cu_7In_4. Obtaining a majority of CIS formation in a film, however, does not necessarily mean we obtained device quality material. In fact, we found, from SEM studies of the processed layered samples, that the films had much too large a surface roughness to be suitable for device fabrication. Figure 11 shows a SEM for the sample of Figure 10.

We also attempted a sample of the same ordering and layer thicknesses

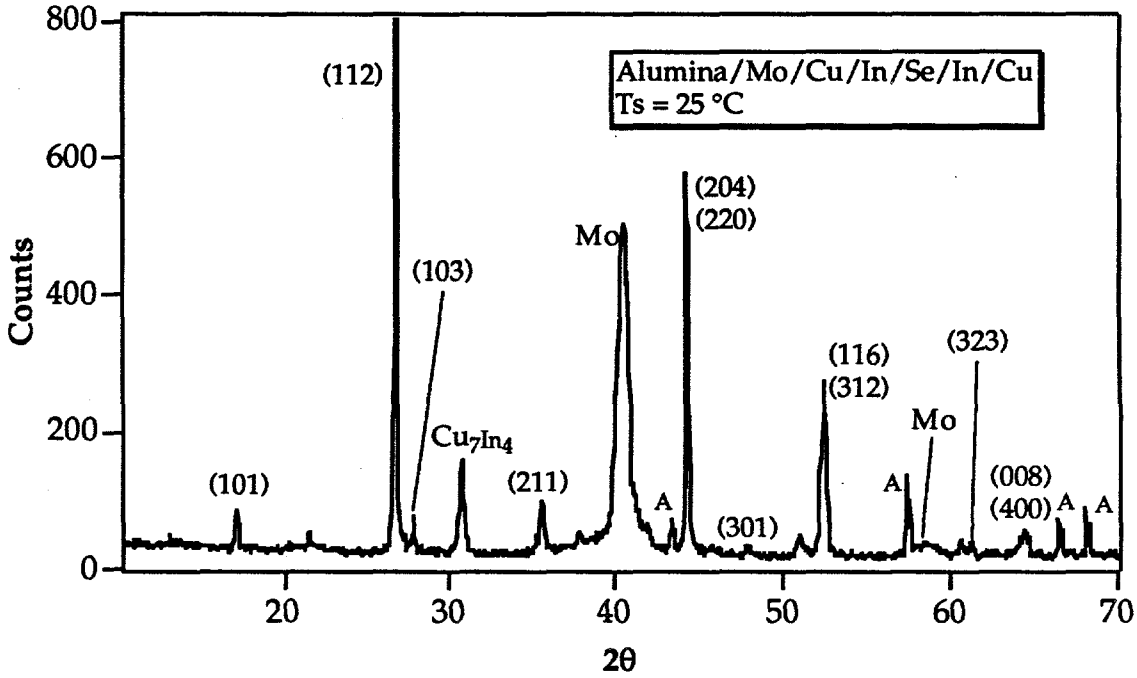

Figure 10. ***XRD Data of a Layered Sample Annealed at 600 °C for 15 Seconds. The Reflections of the (hkl) Panes of CIS are Noted. Ts is the Substrate Temperature During Deposition.***

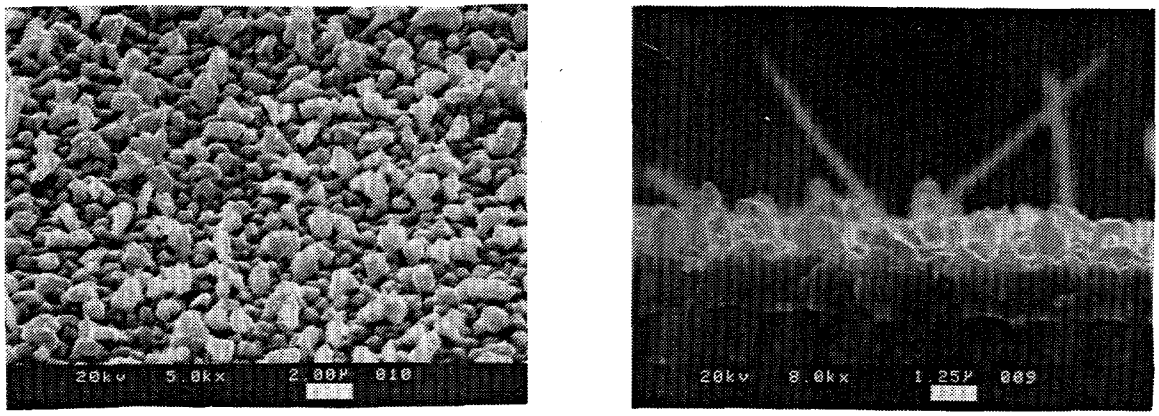

(a) **(b)**

Figure 11. ***Scanning Electron Micrographs of (a) the Surface and (b) the Edge of the Sample of Figure 10.***

deposited at Ts = 170 °C. The results of the processed samples in this case, however, produced films even less suitable for device fabrication. An SEM of a layered sample prepared by this method is shown in Figure 12. Again,

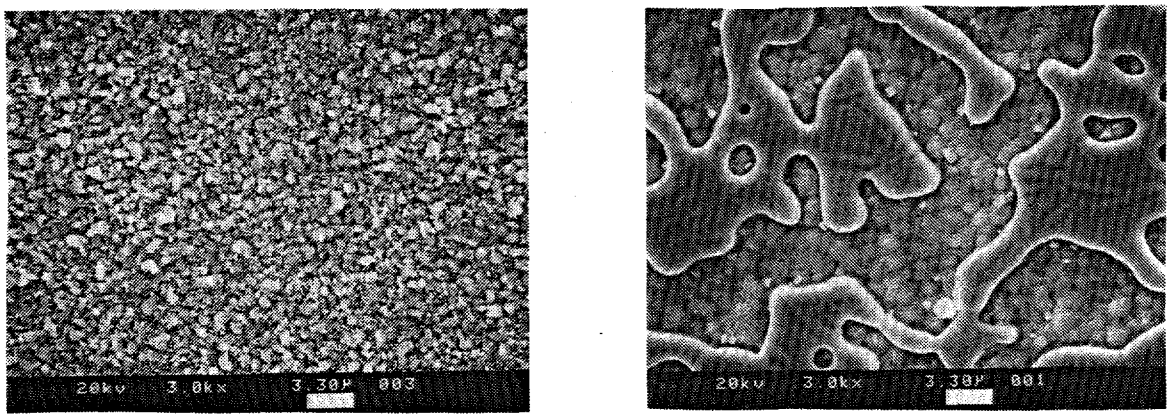

(a) (b)

Figure 12. ***Scanning Electron Micrograph of a Al_2O_3/Cu/In/Se/In/Cu Sample Deposited at Ts = 170 °C. (a) is the Precursor Film and (b) is the Same Sample Processed at 600 °C.***

excessive Se evaporation was responsible for the segregation of the compounds and the large surface roughness. The background matrix had composition 28.00/32.53/21.32/18.16 while the segregated material on the surface had a composition of 63.86/33.32/2.83/0.0. The last number in both cases is the atomic percentage of oxygen present. XRD data of this sample showed a very small amount of CIS formation along with Cu_7In_4, Cu_2O, and In_2O_3.

In order to alleviate the problem of volatilizing Se, we next attempted layered samples of the order Al2O3/Mo/Cu/In/Se/In/Cu/In/Se/In/Cu/In/Se/In/Cu with thickness Al_2O_3/Mo/200/440/1930/440/400/440/1930/440/400/440/1930/440/200Å. These samples were processed under the same

conditions of the previous sample. Control of the composition, resulting from the thin layers, was greatly improved. The composition of a typical processed sample was 23.44/26.25/49.01. Although the sample was Cu-poor, the important point was the lack of Se evaporation. The XRD data in this case showed nearly single phase CIS formation (Figure 13). The surface roughness,

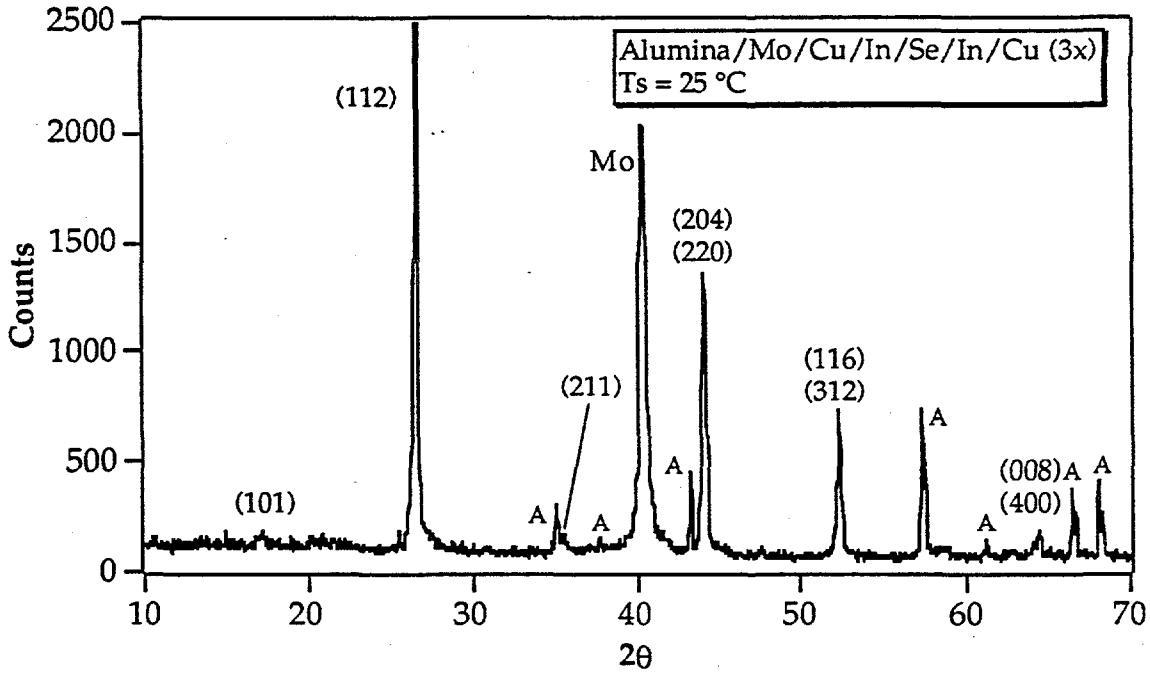

Figure 13. ***Layered Sample Annealed at 600 °C for 15 Seconds.***

as seen in Figure 14, however, was still too large for device fabrication. The surface roughness in this case was a consequence of the deposition, as opposed to an effect of the RTP, as seen by the SEM of the precursor of the same sample.

Preliminary experiments were also performed on co-deposited Cu, In, and Se samples using RTP conditions similar to those used in the layered experiments. These results were very encouraging and will be discussed throughout the rest of this report.

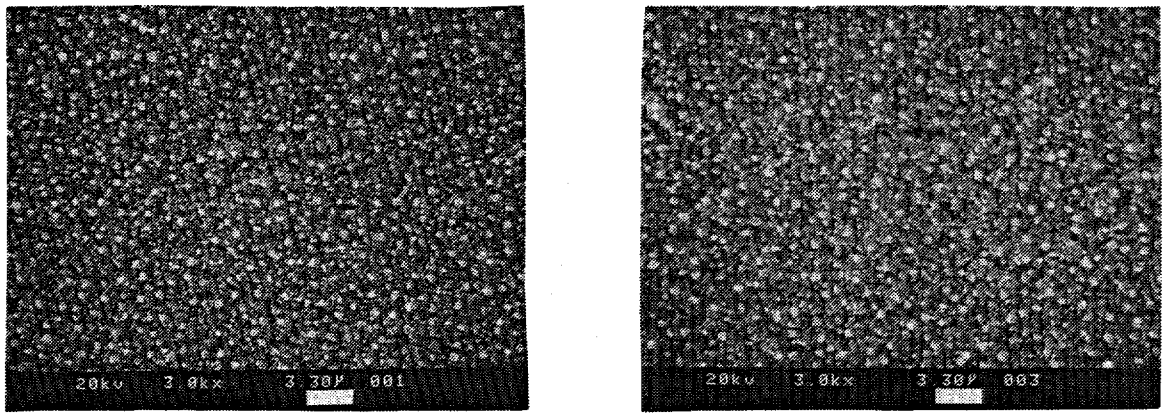

(a) (b)

Figure 14. ***Scanning Electron Micrographs of Al_2O_3/Cu/In (3x) (a) Precursor Deposited at Ts = 170 °C, and (b) the Same Sample Annealed at 600 °C.***

Although the remainder of this initial RTP study will concentrate on co-deposited samples, the layered approach certainly deserves more study, as techniques for the deposition of layers are well developed on an industrial scale (sputtering, electrodeposition). The limited results on processed layered films obtained thus far show much promise. As pointed out above, the number of variables in this experiment is very large. In particular, we feel experiments with the layer ordering may produce films of device quality. It is important to note, however, that the morphology and alloying of the films in this study were strongly dependent on the deposition technique used. Electrodeposition, for example, deposits layers at low temperatures not conducive to alloying. This would result in a precursor with an entirely different morphology and different alloying. We therefore encourage caution in drawing direct analogies between these samples and samples prepared by other methods.

2.2 Rapid Thermal Processing of Co-Deposited Cu, In, and Se Thin Films

Because of the very encouraging preliminary results of the RTP of co-deposited thin films, we chose this type of precursor on which to systematically study the effects of rapid thermal processing on $CuInSe_2$. Based on the preliminary results, we chose to keep constant the variables listed in Table III.

Table III. ***Variables Held Constant in the RTP of Co-Deposited Precursors.***

Variable	Value
•Type of Substrate	Mo coated polycrystalline alumina
•Method of Deposition	Co-deposition of Cu, In, and Se
•Substrate Temperature	225 °C
•Process Atmosphere	Argon
•Intermediate Anneal Steps	0
•Temperature Ramp-Down Rate	Natural cool-down

All precursor films were deposited in a system similar to, but slightly more sophisticated than, the vacuum system discussed in Ref. 2. This system is shown in Figure 15. Accurate co-deposition of the elements is made possible in this system by its rate monitoring capabilities. The copper and indium rates were monitored and controlled by an electron impact emission spectrometer (EIES). This device operates by firing an electron beam into the impinging vapor, causing excitation of electrons in the Cu and In atoms. The subsequent photons emitted are detected by a photomultiplier tube. The number of

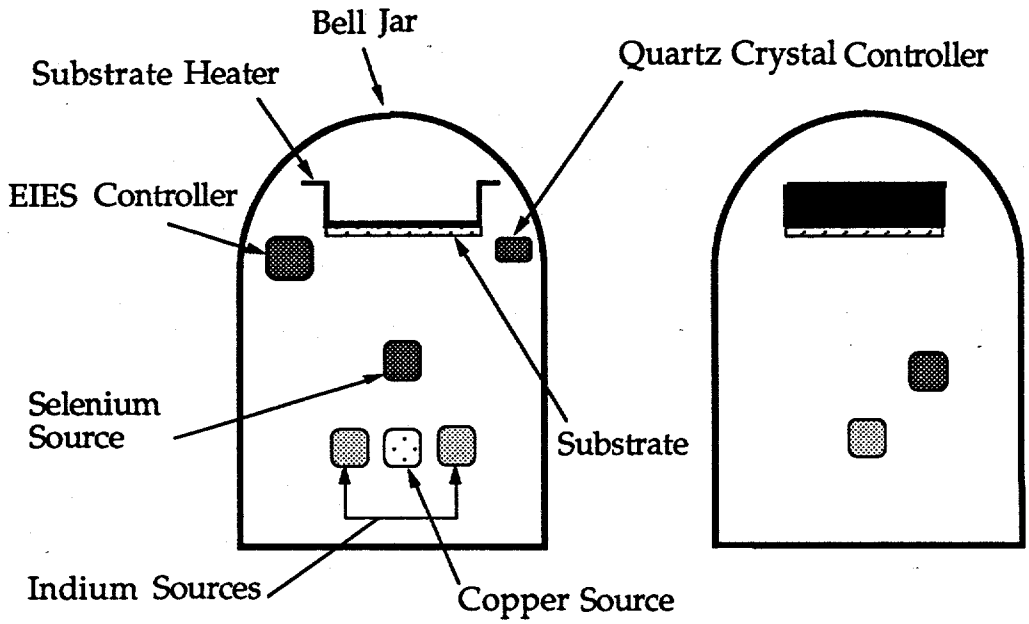

Figure 15. ***Schematic of Vacuum System Used in the Co-Deposition of CIS Thin Film Precursors.***

photons detected that correspond to the spectrum of Cu or In is then converted by the controller to deposition rates. The controller, in turn was interfaced with the evaporation boat current source so that the current was adjusted automatically until the input deposition rate was reached. The Se was controlled in the same manner by a quartz crystal rate monitor as described in Ref. 4. Adequate shielding was in place to prevent the quartz crystal from "seeing" any Cu or In vapor. Filters on the PMT allowed only photons from the atomic spectra of Cu and In to be detected. The structure of a co-deposited precursor is shown in Figure 16.

The variables we chose to explore were the temperature ramp-up rate, the final anneal temperature, and the final anneal time. These parameters were varied systematically in the form of a three-dimensional matrix as shown in

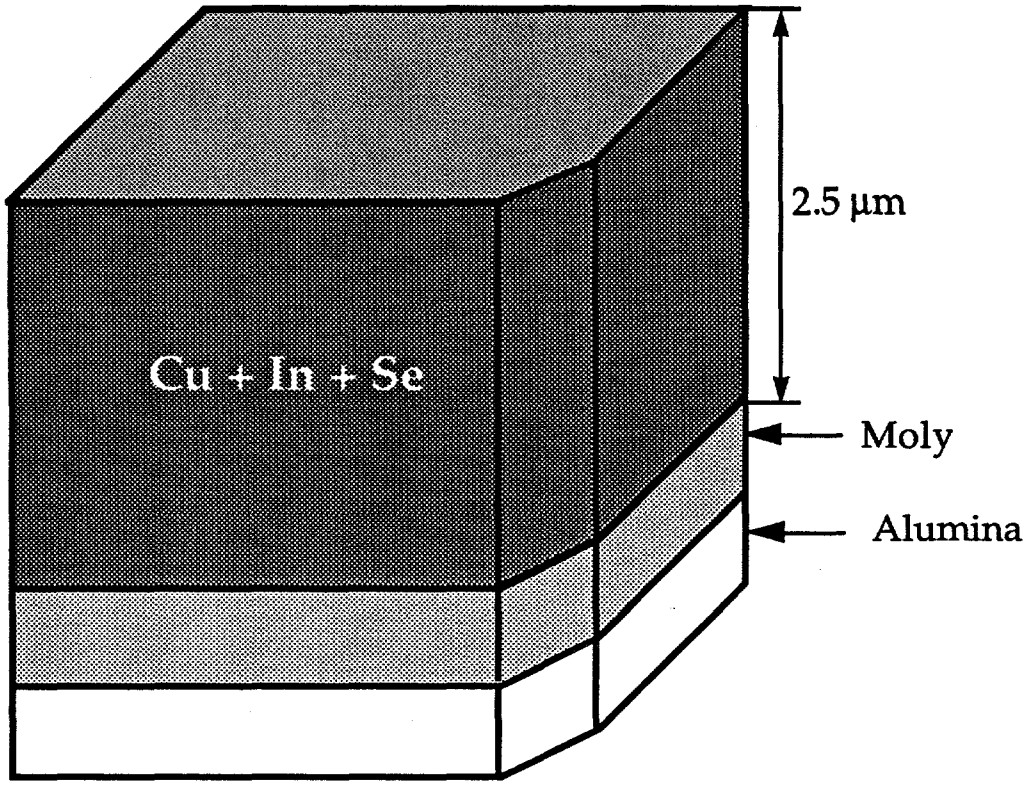

Figure 16. ***Structure of Vacuum Co-Deposited Precursors.***

Figure 17. The ranges chosen in our experimental matrix were based on our preliminary experiments.

The idea behind this type of experimentation was to explore extreme values of the parameter space in an attempt to determine which of the variables under consideration would most positively or negatively affect the results. We therefore performed only the experiments at the corners of the experimental matrix. Corner number one, for example, dictates a process consisting of a temperature ramp-up of 10 °C/s to 500 °C where the final anneal temperature is held for five seconds. Figure 8, for example, shows the anneal profile for corner number six. Data from samples processed at various corners of the experimental matrix are shown throughout the discussion in order to illustrate the versatility of the RTP.

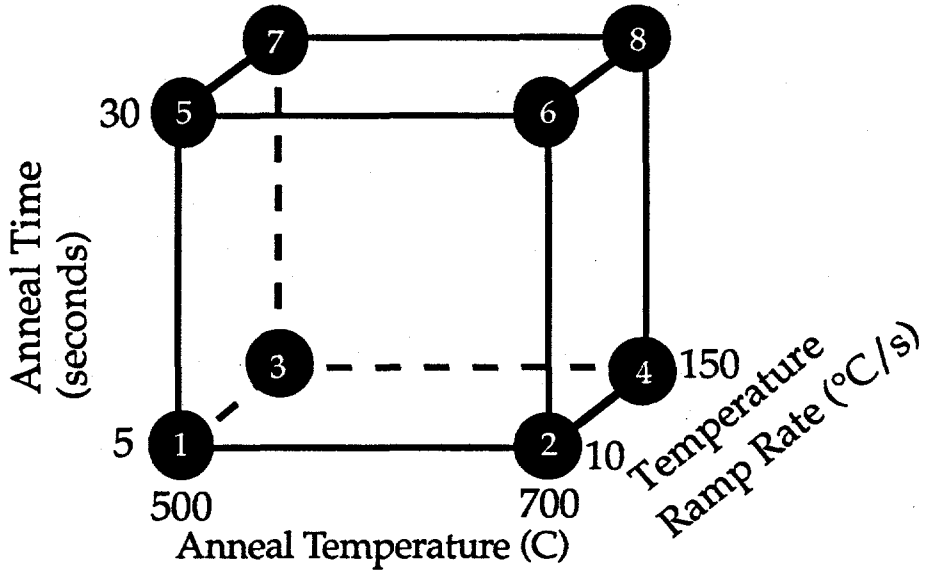

Figure 17. ***RTP Experimental Matrix Showing Parameters Varied and Their Ranges. The Numbers at the Corner Positions are for Reference.***

2.2 i Composition Studies of Co-Deposited CIS Thin Films Formed by RTP

We have performed experiments within this parameter space in three different composition regions – Cu poor (20 at. % Cu), stoichiometric (25 at. % Cu), and Cu rich (28 at. % Cu). These compositions were studied in detail because previous studies of CIS/CdS devices have utilized materials with these compositions [5]. Table IV shows the precursor and post-annealed compositions (as determined by EPMA) for films in the three regions of interest.

The three annealed samples were processed using the conditions at corner seven of Figure 17. There are two important observations to be made from the data in the table. First, because of In-Se binary re-evaporation during the anneal, the films became relatively more Cu rich (Δx increased) in all three regions. This occurred at all annealing conditions and resulted in a need to compensate the

Table IV. ***Comparison of Precursor and Annealed Sample Composition. All Samples Annealed at the Conditions of Corner 7 of Figure 16.***

Composition Region	Precursor Composition (at.% Cu/at.% In/at.% Se)	Annealed Composition (at.% Cu/at.% In/at.% Se)
Cu poor	20.33/27.32/52.35	20.44/27.38/52.04
Stoichiometric	24.36/24.68/50.96	24.94/24.74/50.17
Cu rich	27.03/22.94/50.03	28.81/22.79/48.40

composition of the precursors to obtain the desired post-annealed stoichiometry. Second, we were able to successfully compensate for the material evaporating from the precursors in order to obtain the desired post-annealed stoichiometry. Figures 18 through 23 show the changes in Δx and Δz for samples at the indicated positions of the experimental matrix.

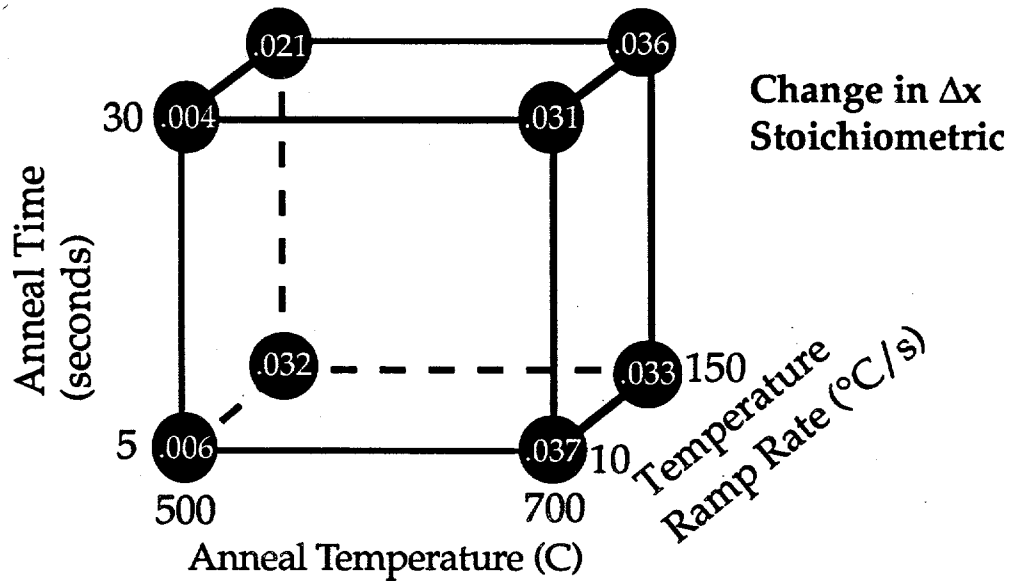

Figure 18. ***The Change in Δx for Stoichiometric Samples Due to the RTP at Conditions Indicated.***

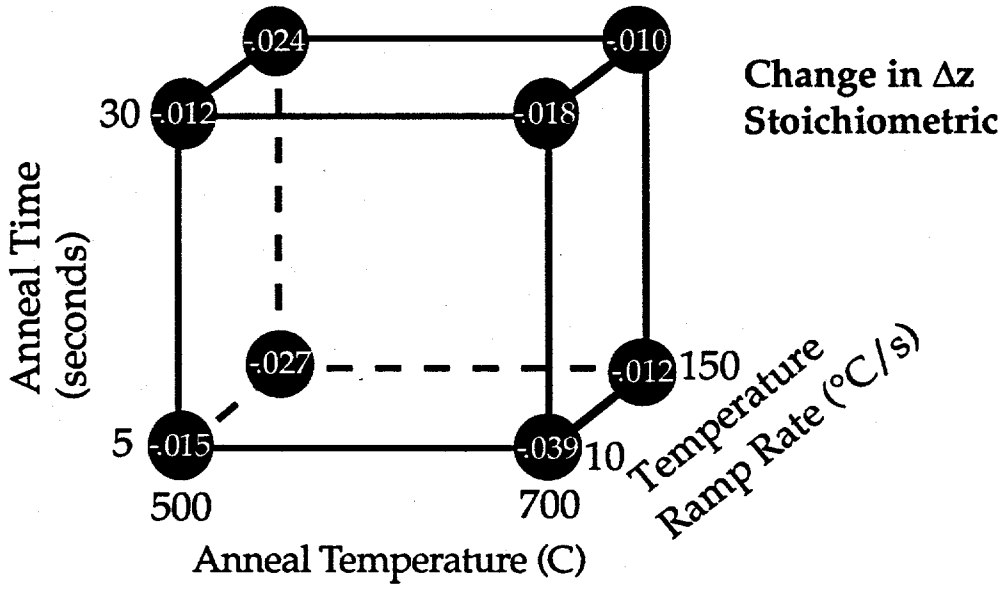

Figure 19. ***The Change in Δz for Stoichiometric Samples Due to RTP at Conditions Indicated.***

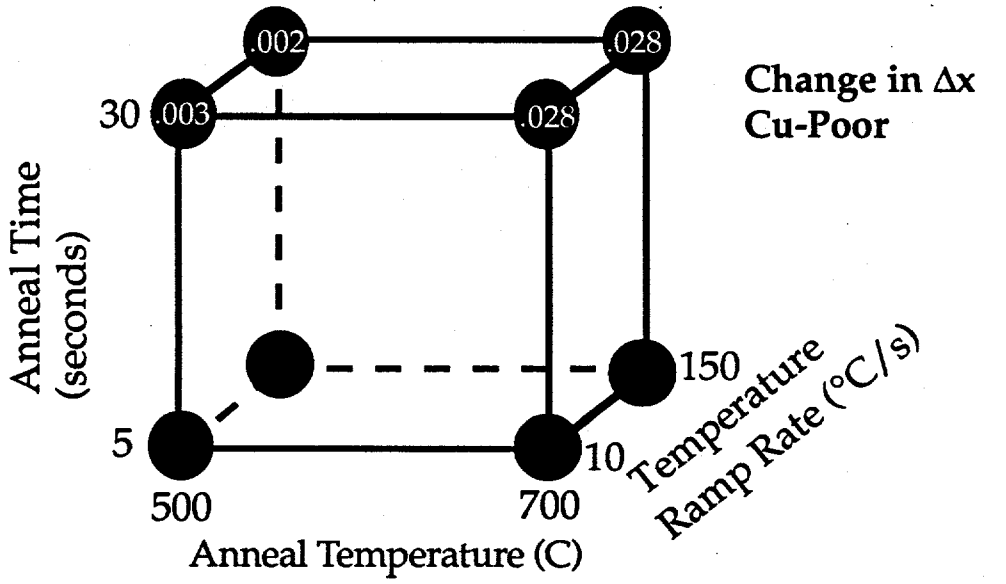

Figure 20. ***The Change in Δx for Cu-Poor Samples Due to RTP at Conditions Indicated.***

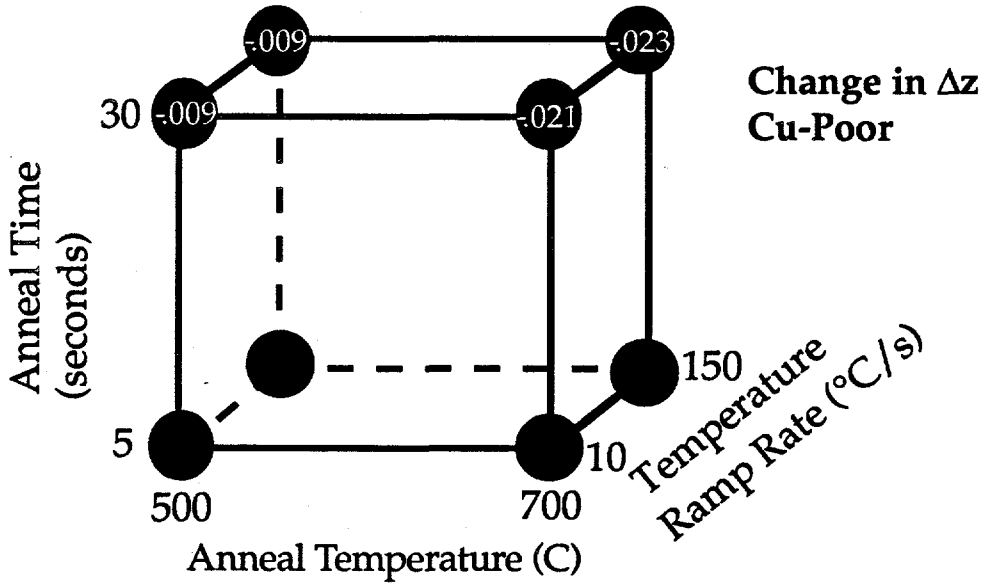

Figure 21. ***The Change in Δz for Cu-Poor Samples Due to RTP at Conditions Indicated.***

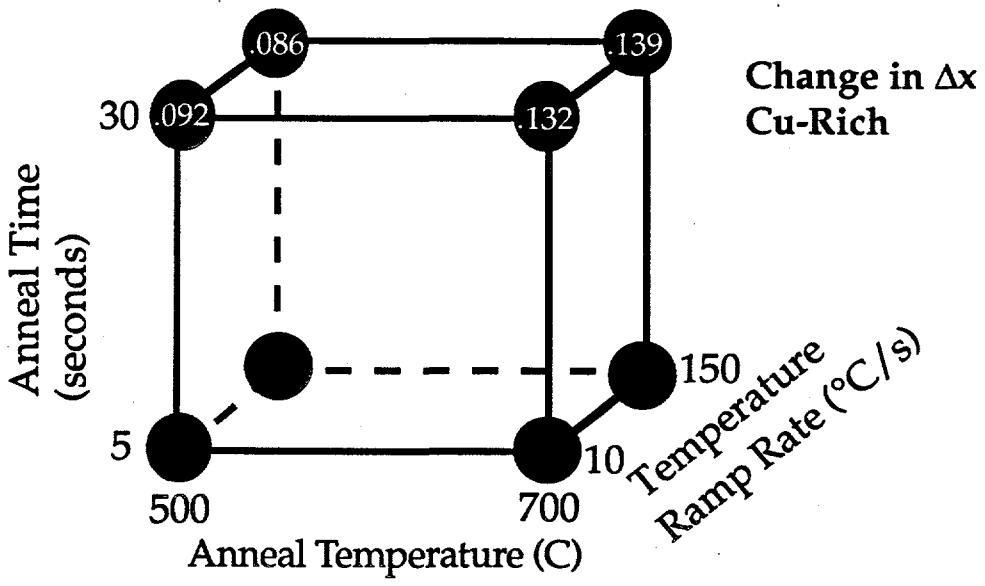

Figure 22. ***The Change in Δx for Cu-Rich Samples Due to RTP at Conditions Indicated.***

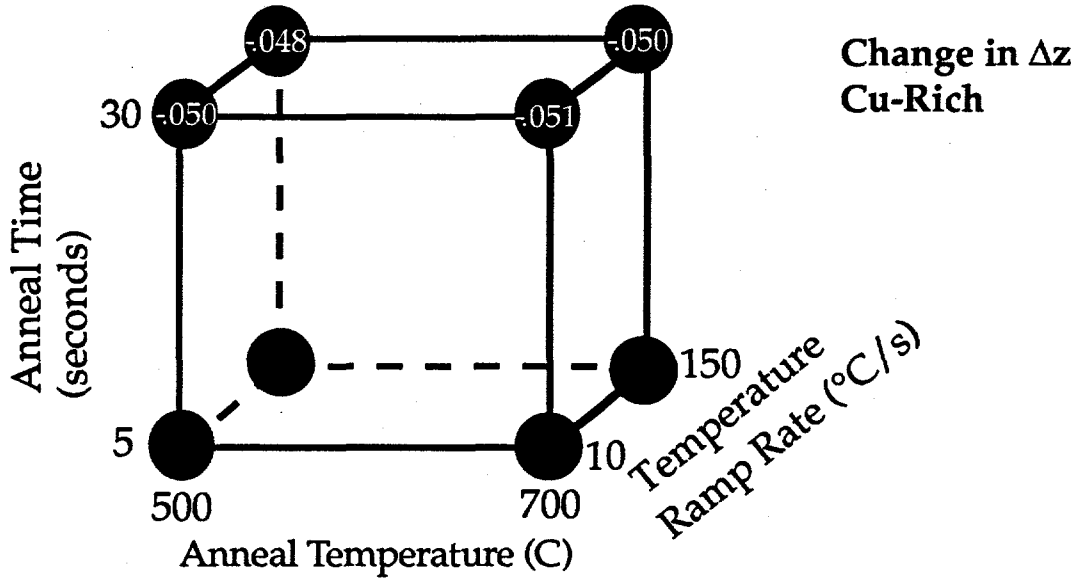

Figure 23. ***The Change in Δz for Cu-Rich Samples Due to RTP at Conditions Indicated.***

The trends from this data are most easily extracted when the change in molecularity and valence stoichiometry is plotted as a function of starting Cu and Se composition, respectively (Figures 24 and 25). Δ(Δx) and Δ(Δz) are

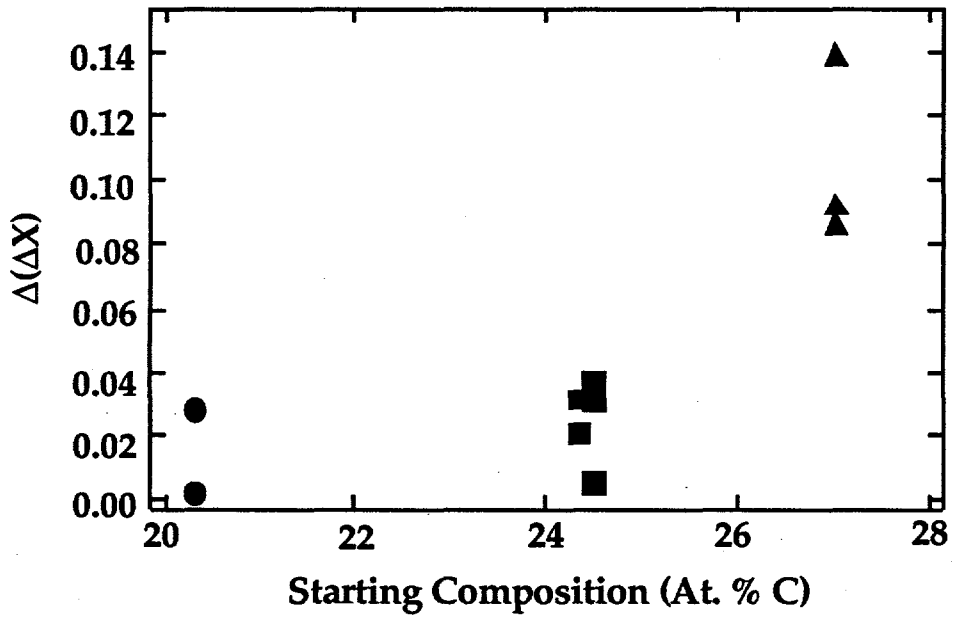

Figure 24. ***The Change in Δx Versus the Starting Atomic Percent Cu for Samples Processed in All Three Composition Regions.***

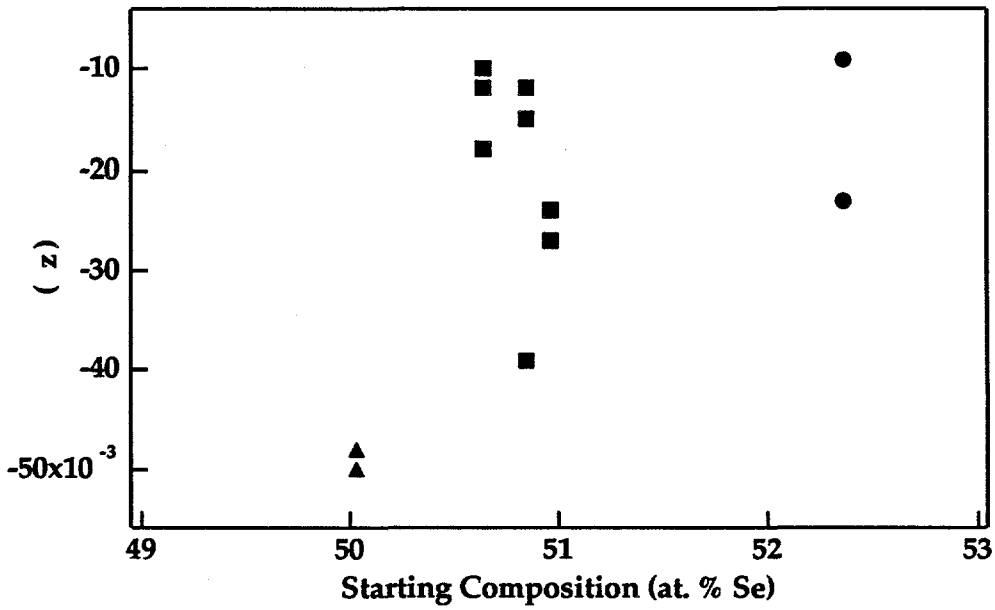

Figure 25. ***The Change in Δz Versus the Starting Atomic Percent Se for Samples Processed in All Three Composition Regions. The Circles Correspond to Cu-Poor Samples, the Squares to Stoichiometric, and the Triangles to Cu-Rich.***

given by equation E-1.

$$\Delta(\Delta x) = \Delta x_{annealed} - \Delta x_{precursor}$$

$$\Delta(\Delta z) = \Delta z_{annealed} - \Delta z_{precursor} \qquad \text{E-1}$$

Two trends are immediately evident. One, every sample becomes more Cu-rich when annealed (Δx increases), and two, every sample loses Se (Δz decreases) when annealed. A closer look at Figures 24 and 25 yields information that begins to give insight into the problem. Specifically, it is seen that the greatest changes in Δx and Δz occur for Cu-rich films. We believe the excess Cu in the Cu-rich films leads to the dominant formation of Cu-Se binaries. These

reactions leave behind Se and In to react to form In-Se binaries that volatilize at around 500 °C (see Ref. 6). This obviously decreases the Se content and increases the Cu/In ratio. Optical and X-ray diffraction analysis to be presented below will support this model and help to form an overall picture of the dynamics of the process.

2.2 ii X-Ray Diffraction Studies of Co-Deposited CIS Thin Films Formed by RTP

Verification of the desired phase of CIS was accomplished by X-ray diffraction (XRD) measurements. The structural properties and theoretical diffraction pattern were discussed in Ref. 7. Diffraction measurements were made with a Rigaku DMAX vertical goniometer and controller system with a rotating Cu-anode X-ray generator. The radiation incident on the sample was Cu-K_α and Cu-K_β with wavelengths of 1.540562 and 1.544390 Å respectively. Data was digitally acquired with DOS based software. The scans had a fixed step width of .05 of a 2θ degree. Data were collected for four seconds at each step. The collected data were analyzed with software purchased from Materials Data, Inc.

Figure 26 shows the XRD pattern of a stoichiometric annealed film processed under the conditions of corner six of Figure 17. As is seen, the film is mostly single phase CIS with the only binary compound detected being the copper selenide peak at a 2θ value of 14°.

Figure 27 shows a comparison of the same film's (112) peak to that of its precursor. In order to meaningfully compare X-ray peak intensities, intensity corrections were performed based on an alumina standard measured before each sample. Figure 28 shows the (112) integrated peak intensities for

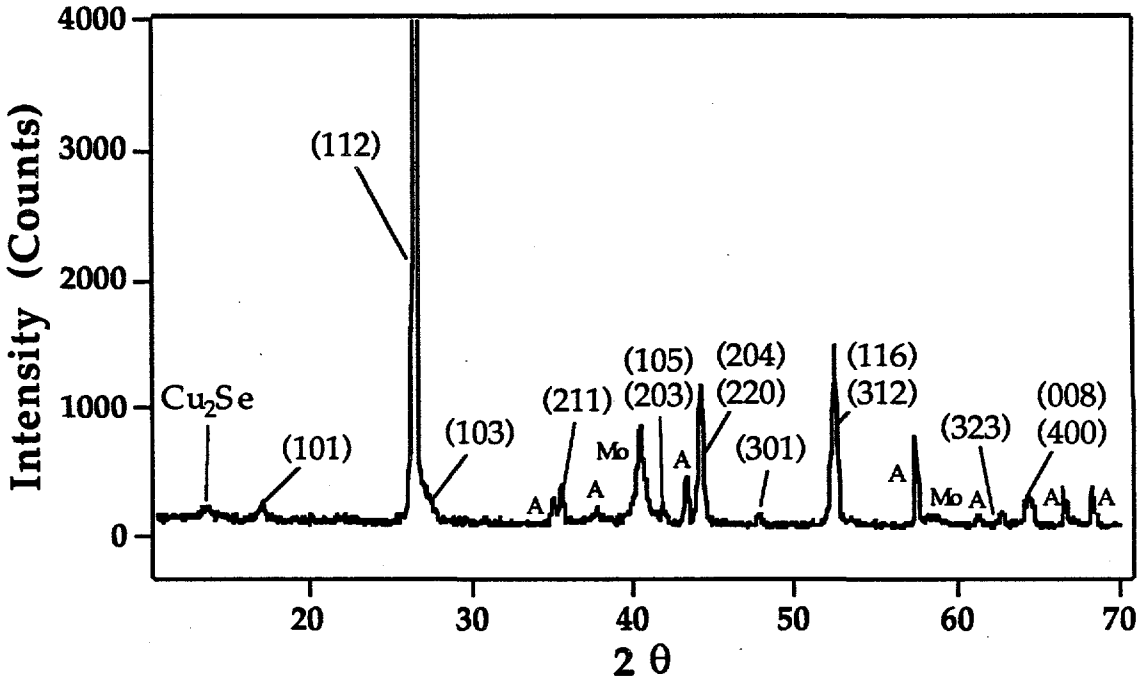

Figure 26. *XRD Data of a Stoichiometric Co-Deposited Sample Anneal Under the Conditions of Corner 6 of Figure 16. The Reflections of the (hkl) Planes of CIS are Noted. The "A"s Denote Alumina Peaks.*

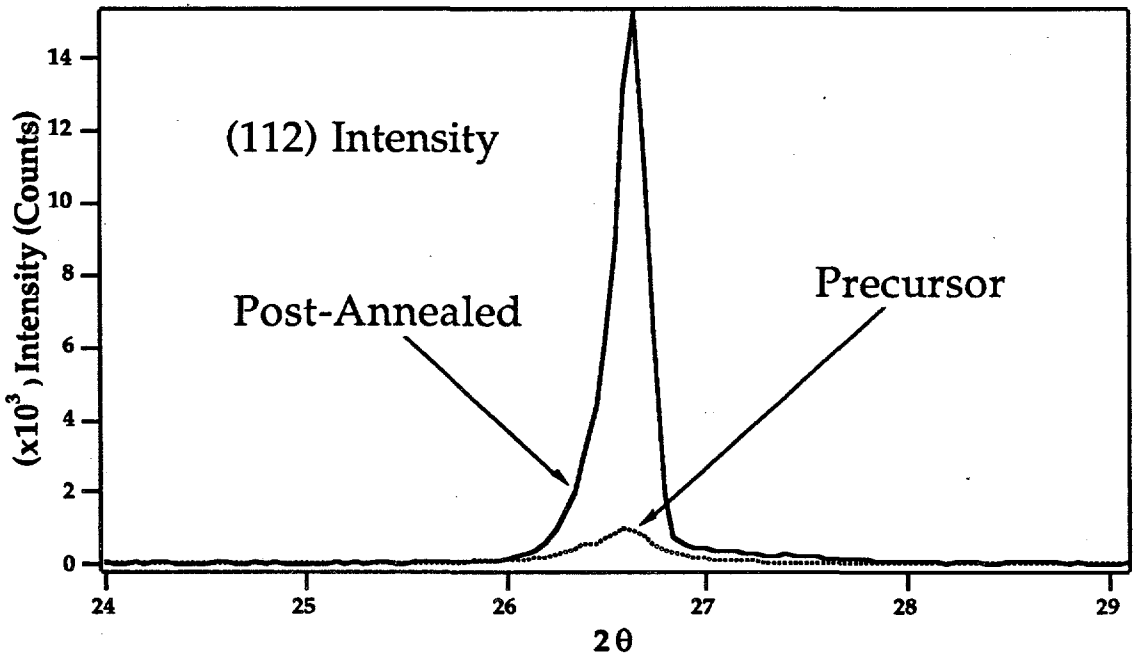

Figure 27. *XRD Data Comparing (112) Peak Intensities of the Film of Figure 24 and its Precursor. Significant Recrystallization is Evident.*

stoichiometric samples processed under the RTP conditions shown. Analysis of this figure indicates the general trend is higher temperatures, longer anneals and slower temperature ramp rates result in larger volume recrystallization. This trend was also evident in recrystallized Cu-poor and Cu-rich films.

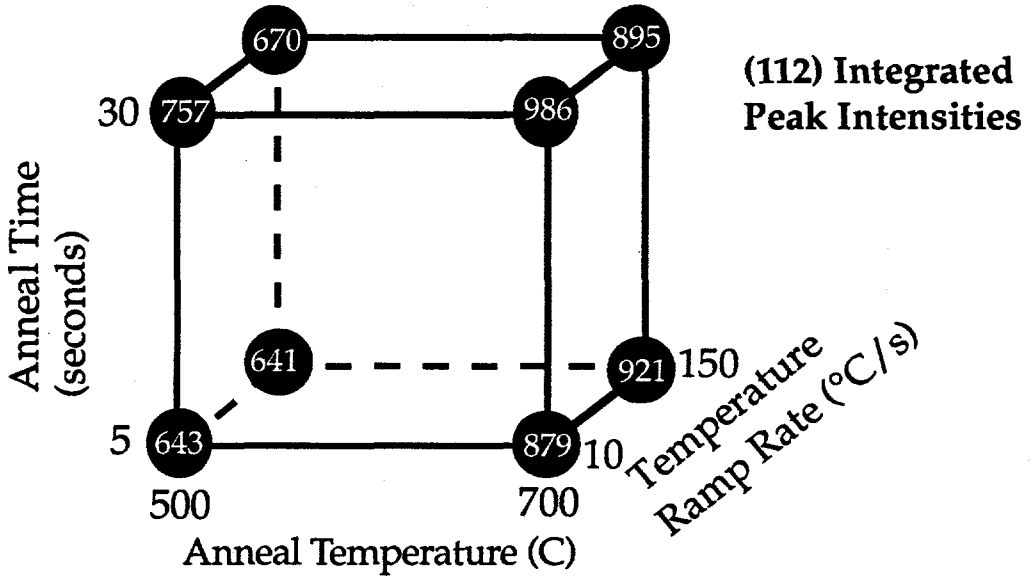

Figure 28. ***(112) Integrated Peak Intensities for Films Processed at the Conditions Shown.***

Figures 29 and 30 show the XRD results for a recrystallized Cu-poor and Cu-rich film respectively. Figure 29 indicates a majority of CIS formation. Also present in the Cu-poor film XRD data were the signature peaks of Cu_2Se at 14°, In_2Se_3 at 25°, $Cu_{.22}In_{1.25}Se_{3.5}$ at 39°, and the ordered vacancy compound (OVC) whose peaks are convoluted with the primary CIS peaks. The OVC is phase of CIS present in Cu-poor materials given by $CuIn_2Se_{3.5}$. The OVC exhibits tetragonal symmetry with an ordered In sublattice and associated Cu vacancies.

Figure 30 also shows a large volume of CIS formation. In this case, the

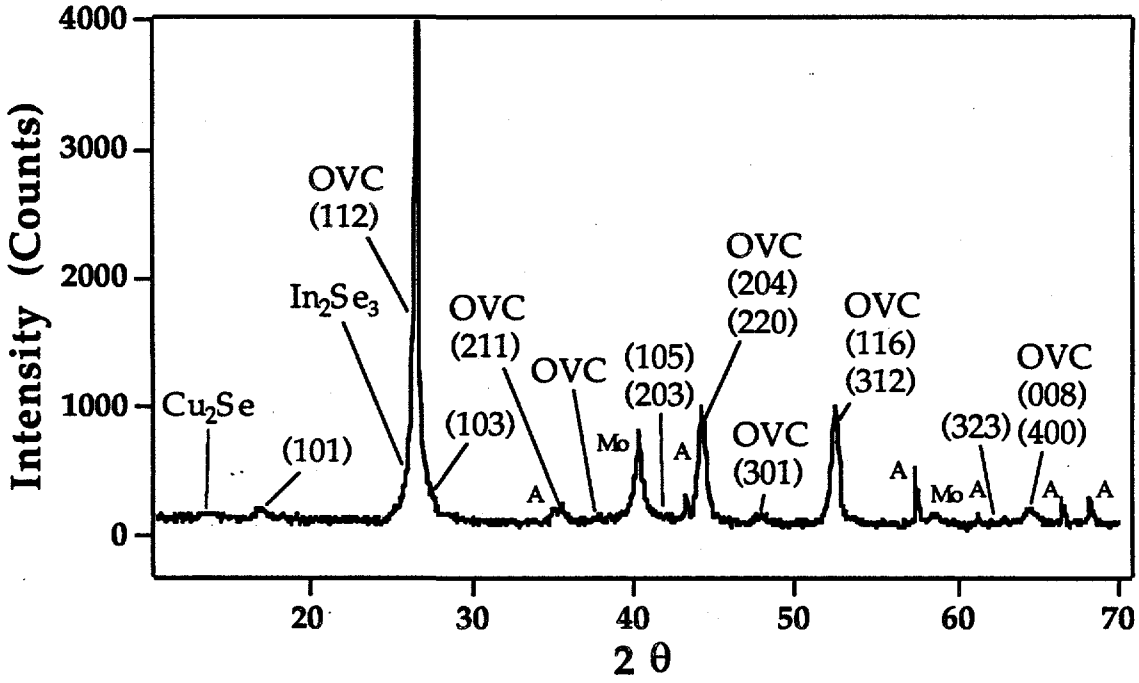

Figure 29. *XRD Data of a Cu-Poor Sample Processed at Corner 6 of the Experimental Matrix. OVC Indicates the Ordered Vacancy Compound.*

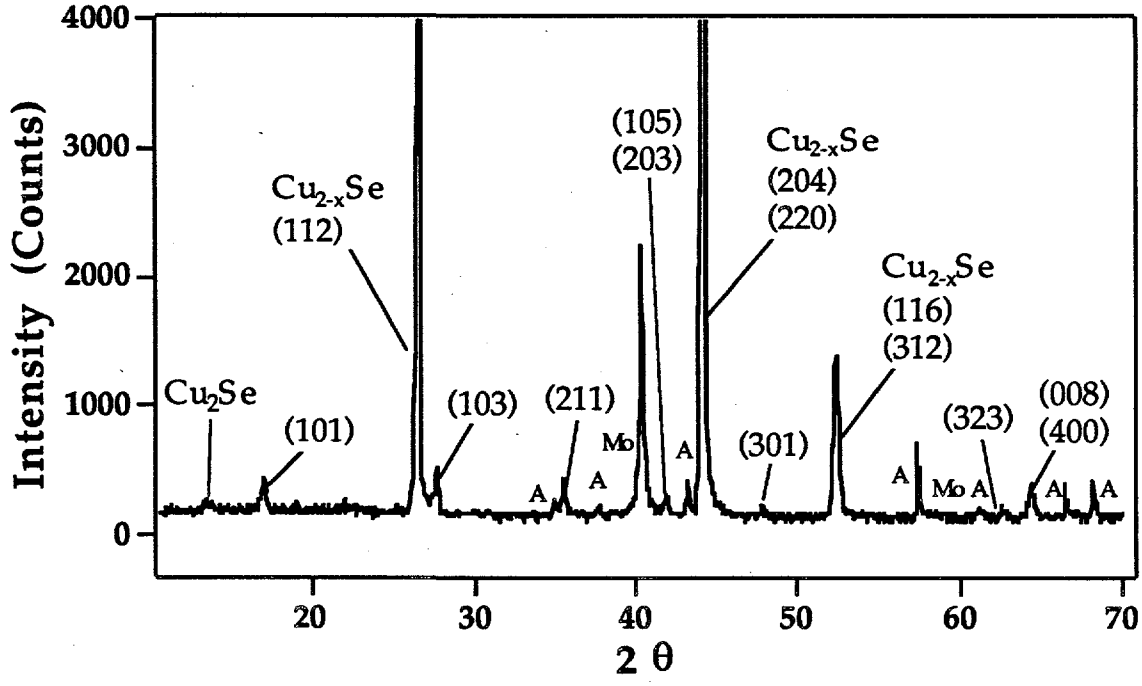

Figure 30. *XRD Data of a Cu-Rich Sample Processed at Corner 6 of the Experimental Matrix.*

excess Cu concentrations result in a large volume of Cu_2Se and $Cu_{2-x}Se$ formation as well. As indicated in the figure, the $Cu_{2-x}Se$ peaks are convoluted with the CIS peaks. The primary peak of the $Cu_{2-x}Se$ phase is convoluted with the (202)/(220) CIS peak, which explains the increased intensity of this peak relative to the (112) peak. It should be noted that the XRD results from all three composition regions agree with published data [8] for vacuum deposited films reacted *in-situ* by elevated substrate temperatures. The X-ray diffraction patterns for the remainder of the samples processed under the conditions of the experimental matrix are shown in Appendix B of Ref. 9.

Several important conclusions can be drawn from the X-ray diffraction data. Most important, we have demonstrated the ability to fabricate CIS thin films using post-deposition processing times of less than two minutes. Further, the films have the expected tetragonal syemmetry of the chalcopyrite structure and are comparable to films fabricated by more lengthy, conventional thermal anneals. Also, the X-ray data is consistent with the data of the composition study presented above, with the data for the Cu-rich films showing significant Cu-Se binary formation, which leads to the formation of the easily volatilized In-Se compounds.

2.2 iii Optical Studies of Co-Deposited CIS Thin Films Formed by RTP

Typically, the experimentally determined optical properties of semiconducting thin films are presented in terms of the absorption coefficient α. However, there exists no method by which to experimentally determine α directly. In this section, we will give some general background of the optical properties of semiconductors (after References 10 and 11), discuss the method

used in this study to determine α, and present the experimental results of our films.

2.2 iii (a) General Theory of the Optical Properties of Semiconductors

As mentioned, when discussing the optical properties of thin film semiconductors, the experimental data is typically presented in terms of the absorption coefficient α. α is defined as the decrease in intensity, I, of the incident radiation as a function of distance into the film. α is a function of photon energy and can be expressed as

$$\alpha(h\nu) = \frac{1}{I(h\nu)} \frac{dI(h\nu)}{dx}, \qquad \text{E-2}$$

where ν is the frequency of the radiation, and hν is the photon energy. α can also be expressed as a function of the probability that a photon will excite an electron from a given initial state n_i, to a given final state n_f.

$$\alpha(h\nu) = A\Sigma P_{if} n_i n_f \qquad \text{E-3}$$

As discussed in Ref. 12, CIS is a direct band-gap material. We will therefore proceed with the discussion from this standpoint assuming that all valence band states are full and that all conduction band states are empty, which is the case for 0 °K. As we know from our discussions in Ref. 13, for a direct transition $h\nu = E_f - E_i$. Referring to Figure 2-2 of Ref. 14, for an allowed transition from band edge to band edge, we can express the energies of the initial and final states in terms of the energy gap, momentum, and the electron and

hole effective masses.

$$E_i = \frac{h^2k^2}{4\pi^2 m_h^*} \qquad \text{E-4}$$

$$E_f - E_g = \frac{h^2k^2}{4\pi^2 m_e^*}$$

Adding these two expressions yields

$$h\nu - E_g = \frac{h^2k^2}{4\pi^2}\left(\frac{1}{m_e^*} + \frac{1}{m_h^*}\right). \qquad \text{E-5}$$

The density of states available for transitions due to photons of energy hν can be obtained by considering equation E-5 with a slight modification of equation 2-4 [14].

$$N(h\nu)\, d(h\nu) = \frac{4\pi(2m_r^*)^{3/2}}{h^3}(h\nu - E_g)^{1/2}\, d(h\nu) \qquad \text{E-6}$$

where $m^*_r = 1/m^*_e + 1/m^*_h$ and is known as the effective reduced mass. The integral given by equation 2-3 [14] will then give a number proportional to the number of photons absorbed. This in turn leads to an expression for α.

$$\alpha(h\nu) = A^*(h\nu - E_g)^{1/2} \qquad \text{E-7}$$

where A* is given by [15]

$$A^* \approx \frac{q^2\left(2\frac{m_e^* m_h^*}{m_e^* + m_h^*}\right)}{nch^2 m_e^*}. \qquad \text{E-8}$$

In this equation, n = index of refraction, q is the electron charge, and c is the speed of light. Observation of equation E-7 shows us that if α^2 is plotted versus the incident photon energy hν, the fundamental absorption will be linear. Furthermore, extrapolation of the α^2 curve to the photon energy axis intercept will yield the band-gap of the material. This is equivalent to setting $\alpha = 0$ in equation E-6 and solving for E_g. Also, since $h\nu - E_g$ is linear in α^2, the slope of the line is given by A*. Determination of the slope then yields information about the effective masses.

2.2 iii (b) Experimental Determination of the Optical Properties of CIS.

The method used in this study to determine α is to relate the measured values of the total reflectance, total transmittance, and film thickness to the index of refraction ($n_c = n - ik$). In this expression, $k=\alpha\lambda/4\pi$, and is known as the extinction coefficient. λ is the wavelength of the incident radiation. The reflectance, R, and transmittance, T, are given by

$$R = \frac{(n-1)^2 + k^2}{(n+1)^2 + k^2}$$

$$T = \frac{(1-R)^2 e^{-\alpha x}}{1 - R^2 e^{-2\alpha x}}. \qquad \text{E-9}$$

One method commonly used to determine α is to consider the reflectance and transmittance at the interfaces of the entire system (Figure 31). Based on this

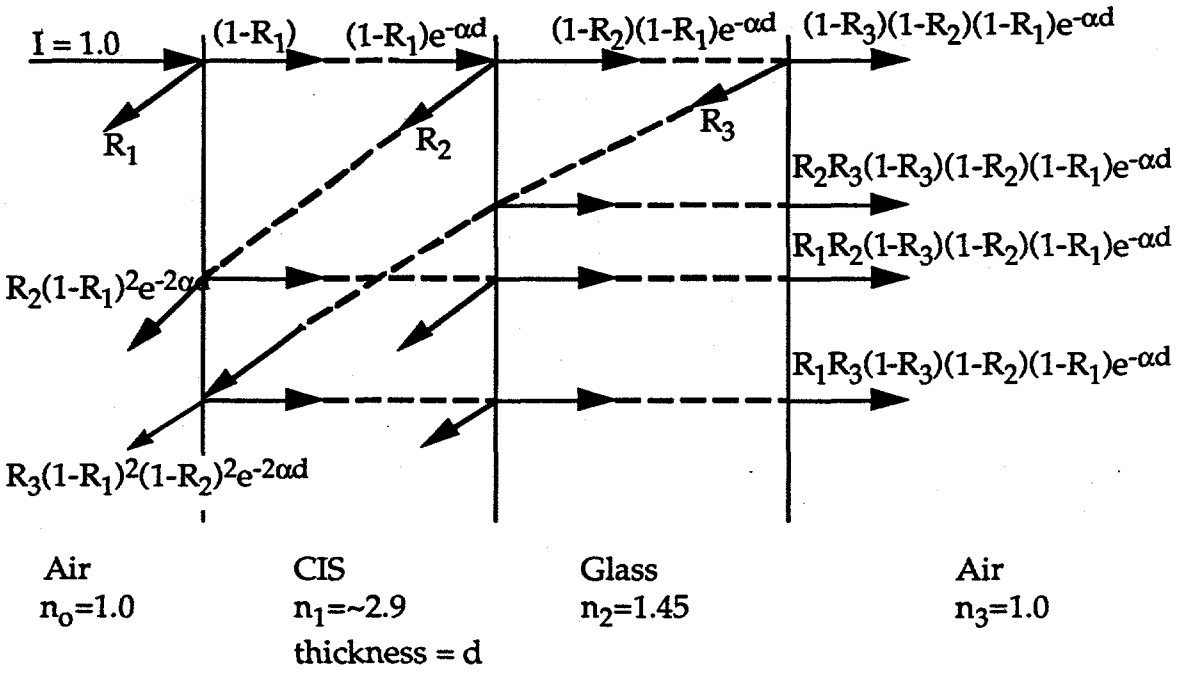

Figure 31. ***Reflection and Transmission Model for Air/CIS/Glass/Air System. (After Reference 16.)***

model, Denton et al. have developed a method to calculate α based on the measured R and T, and the measured film thicknesses as they relate to the Fresnel coefficients, $f_1(n,k)$ and $f_2(n,k)$ [17]. These are given by

$$f_1(n_1,k_1) = \left(\frac{1+R}{T}\right) = \left(\frac{1}{4n_o n_2(n_1^2+k_1^2)}\right)\left\{(n_o^2+n_1^2+k_1^2)\left[(n_1^2+n_2^2+k_1^2)\cosh(2\alpha t)+2n_1n_2\sinh(2\alpha t)\right]\right.$$
$$\left. + (n_o^2-n_1^2-k_1^2)\left[(n_1^2-n_2^2+k_1^2)\cos\left(\frac{4\pi n_1 t}{\lambda}\right) - 2n_2k_1\sin\left(\frac{4\pi n_1 t}{\lambda}\right)\right]\right\} \qquad \text{E-10}$$

$$f_2(n_1,k_1) = \left(\frac{1-R}{T}\right) = \frac{1}{2n_2(n_1^2+k_1^2)}\left\{n_1\left[(n_1^2+n_2^2+k_1^2)\sinh(2\alpha t) + 2n_1n_2\cosh(2\alpha t)\right]\right.$$
$$\left. + k_1\left[(n_1^2-n_2^2+k_1^2)\sin\left(\frac{4\pi n_1 t}{\lambda}\right) + 2n_2k_1\cos\left(\frac{4\pi n_1 t}{\lambda}\right)\right]\right\} \qquad \text{E-11}$$

where t is the thickness of the CIS film. The other variables are given in Figure 31. A careful accounting of these equations shows that all the variables are either known or measured except α.

The R and T data were collected using a Beckman 5240 spectrophotometer equipped with an integrating sphere. Data were taken digitally with a Macintosh SE computer over the wavelength range of 2200 to 750 nm in 4 nm increments. A normalization was then performed using data from a $BaSO_4$ standard obtained from the National Institute of Standards and Technology to compensate for losses in the $BaSO_4$ on the walls of the integrating sphere. The absorption coefficient was calculated by computer using software written by co-workers at SERI (J. Tuttle). The calculations were done based on the input value of n, which was taken to be constant at 2.9 [18]. The films were deposited on Corning 7059 glass to a thickness of ~ 5000Å. The thickness input for the calculations was determined by a Tencor thin-film profilometer. This thickness range was chosen in order to obtain accurate transmission data.

Optical reflection and transmission measurements were taken on co-deposited stoichiometric, Cu-poor, and Cu-rich films that were processed under the conditions shown in Figure 17. From this data, the absorption coefficient α was calculated as discussed above, and for the processed films was on the order of 5×10^4 cm^{-1}. A plot of the log of alpha versus photon energy is shown in Figures 32, 33, and 34 for stoichiometric, Cu-poor, and Cu-rich films respectively, and their precursors. All three samples were processed under the conditions of corner eight in Figure 16. As is seen, the processed stoichiometric film has very little sub-gap absorption and the transition is very sharp, indicating a direct valence to conduction band transition with minimum allowed impurity states in the gap. The Cu-poor sample has slightly more sub-gap absorption,

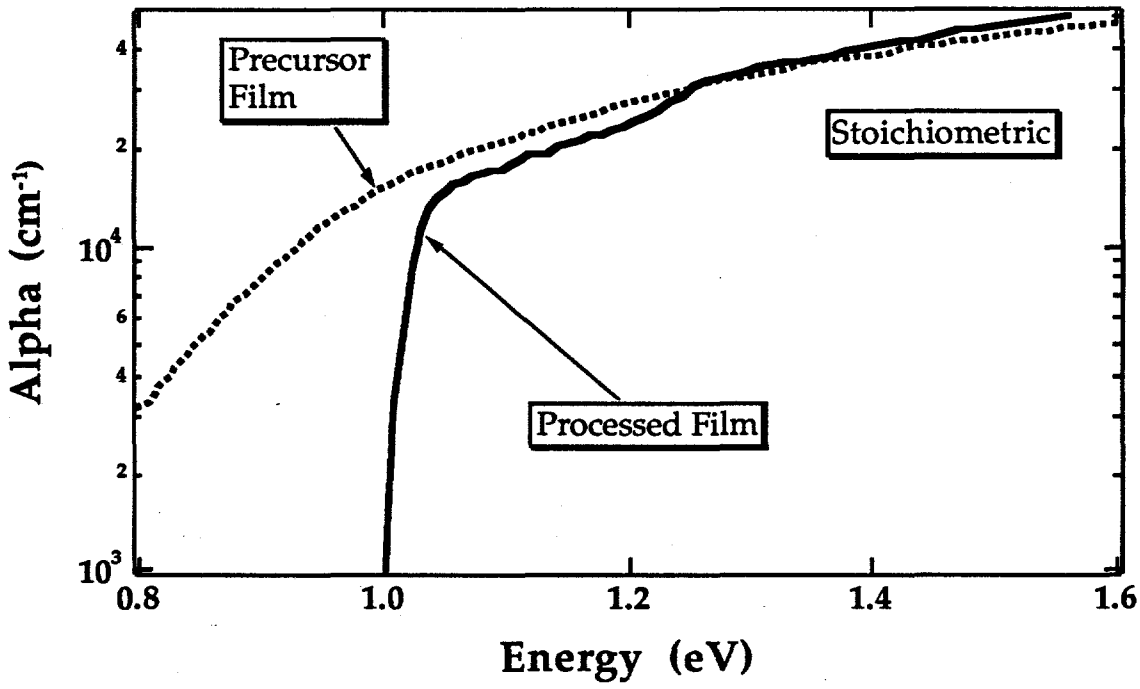

Figure 32. *Plot of Log of α Versus Incident Photon Energy for a Co-Deposited, Stoichiometric Sample Processed Under the Conditions of Corner 8 and its Precursor.*

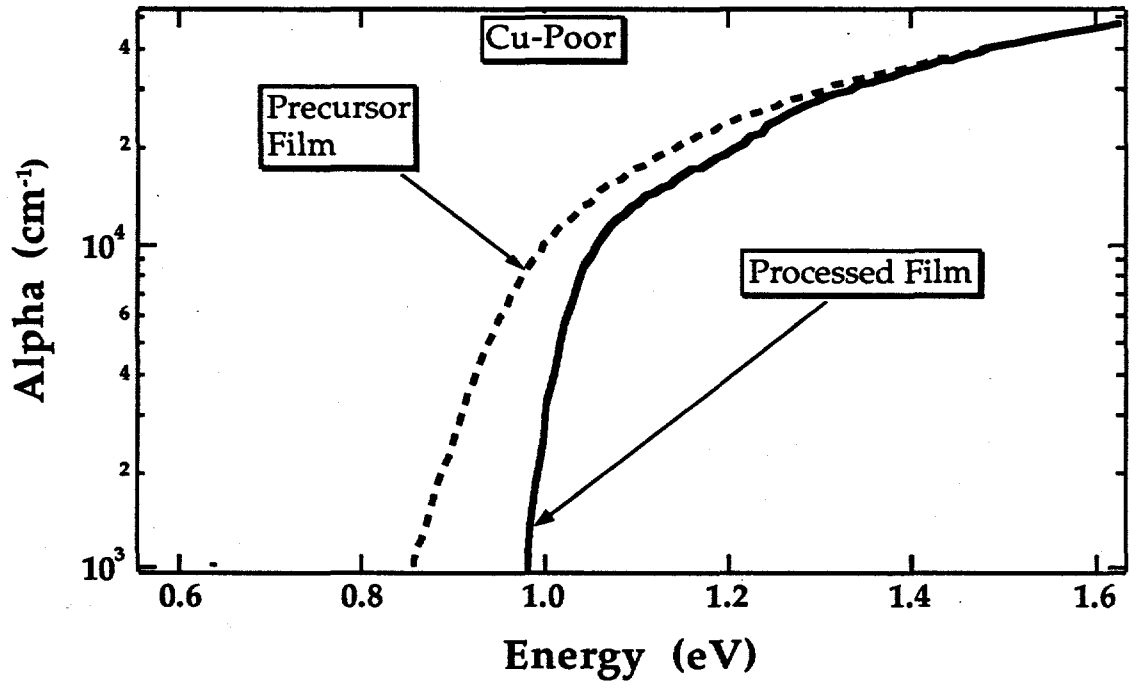

Figure 33. *Plot of Log of α Versus Incident Photon Energy for a Co-Deposited, Cu-Poor Sample Processed Under the Conditions of Corner 8 and its Precursor.*

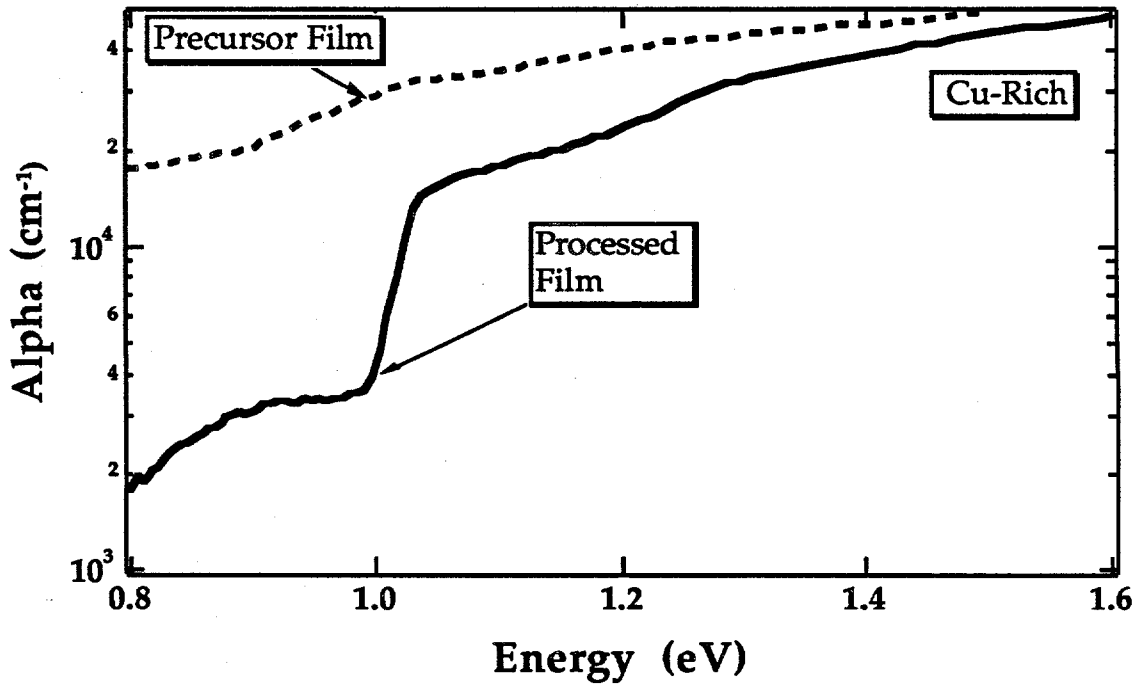

Figure 34. ***Plot of Log of α Versus Incident Photon Energy for a Co-Deposited, Cu-Rich Sample Processed Under the Conditions of Corner 8 and its Precursor.***

absorption, indicating the existence of more states in the gap than the stoichiometric sample. The Cu-rich sample, on the other hand, has sub-gap absorption on the order of $3x10^4$ cm^{-1} indicating the existence of many impurity states in the gap. Differences in all processed samples showed similar results except for the stoichiometric sample processed under the conditions of corner three of the experimental matrix. Figure 35 shows a comparison of the film, its precursor, and the processed film shown in Figure 32. The data for the remaining samples is shown in Appendix C of Ref 19.

When studying the results of the composition study, the X-ray analysis, and the optical data, certain correlations became apparent. Starting with the Cu-poor material, the composition study showed only small changes in Δx and Δz. Based on our model that evaporating binaries are responsible for these

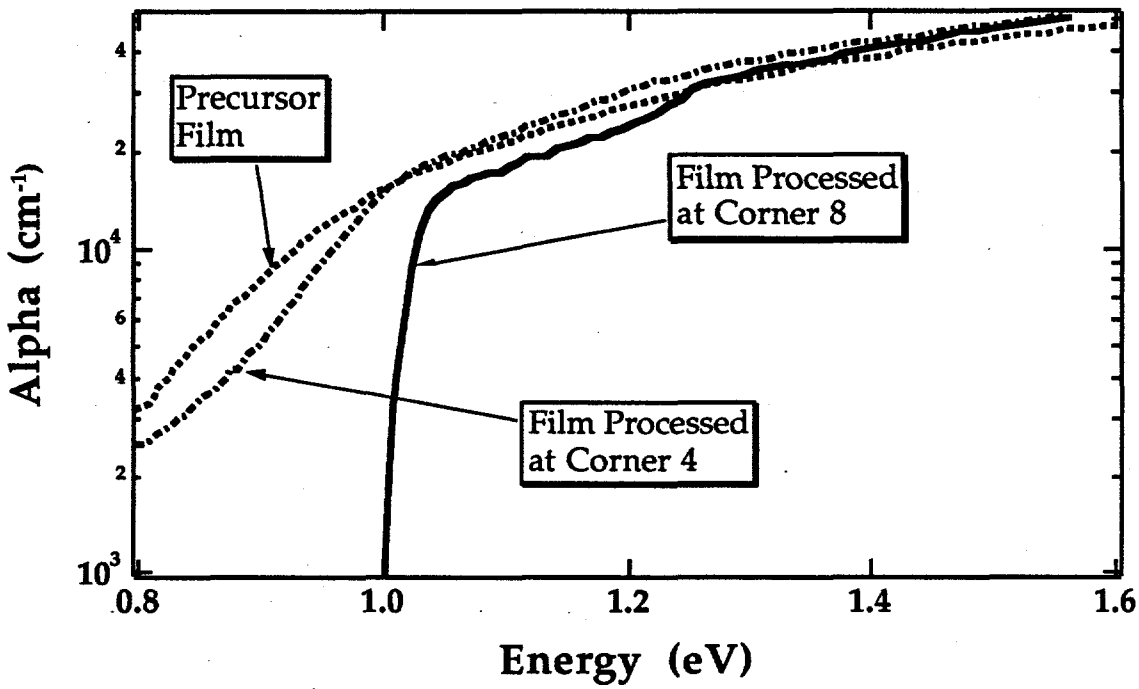

Figure 35. ***Plot of Log of α Versus Incident Photon Energy for a Co-Deposited, Stoichiometric Sample Processed Under the Conditions Indicated and their Precursors.***

changes, small changes would indicate little binary formation in the precursor. The XRD data of the annealed Cu-poor film supports this in that there is very little binary incorporation in any of these films. The optical data strongly support this contention. The absorption of the precursor film shows a relatively sharp transition, indicating significant CIS formation. This being the case, little material is left for the formation of the easily volatilized binaries.

This trend continues with the stoichiometric films. The composition study revealed slightly larger changes in Δx and Δz, indicating more evaporation of binaries. The X-ray data for these films showed more Cu-Se formation. This is supported by the absorption data, which shows more sub-gap absorption indicating less CIS formation in the precursor film. If less CIS forms, this leaves more unreacted material to form the more volatile binaries.

In the copper rich samples, the data shows that the reaction in the

precursors is dominated by Cu-Se binaries. The Cu-rich samples have the largest Δx and Δz, changes indicating significant material evaporation during processing. This is consistent with the XRD data, which shows a large amount of $Cu_{2-x}Se$ incorporation in the film. And finally, the optical data strongly supports our model. The Cu-rich precursor data is identical to absorption data published for $Cu_{2-x}Se$ thin films [17]. Considering the atomic ratios of the material deposited, $Cu_{2-x}Se$ formation would leave a significant amount of Se and almost all the In unreacted, which would form easily volatilized In-Se binaries. The large amount of sub-gap absorption in the Cu-rich films is attributed to the $Cu_{2-x}Se$ binary remaining in the processed film.

Composition dependent trends are also evident when α^2 is plotted versus incident photon energy. Figures 36, 37, and 38 show these results for the stoichiometric, Cu-poor, and Cu-rich samples respectively. The band-gap was

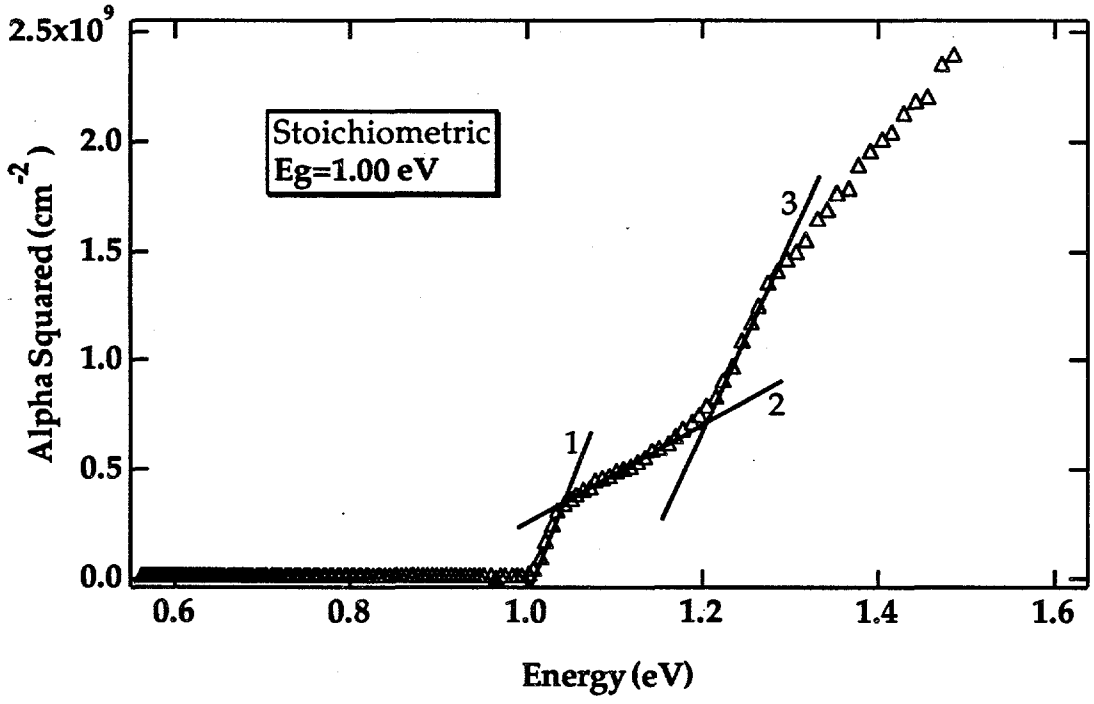

Figure 36. *Plot of α^2 Versus Incident Photon Energy for a Co-Deposited, Stoichiometric Sample Processed Under the Conditions of Corner 8. The Transitions are Numbered for Reference.*

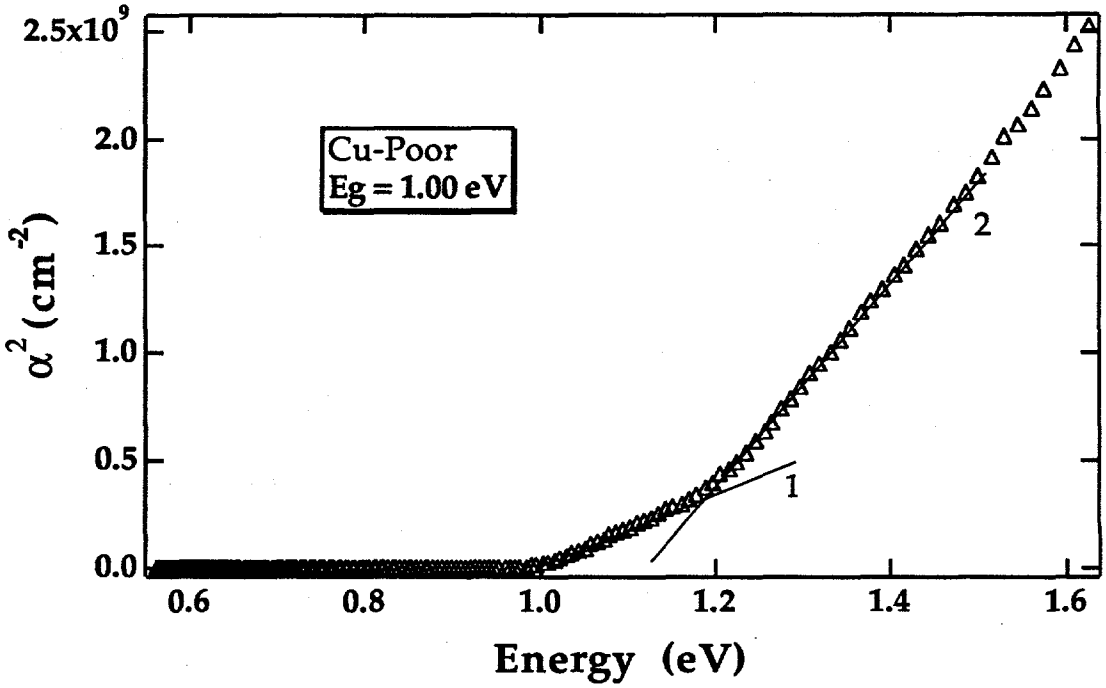

Figure 37. *Plot of α^2 Versus Incident Photon Energy for a Co-Deposited, Cu-Poor Sample Processed Under the Conditions of Corner 8. The Transitions are Numbered for Reference.*

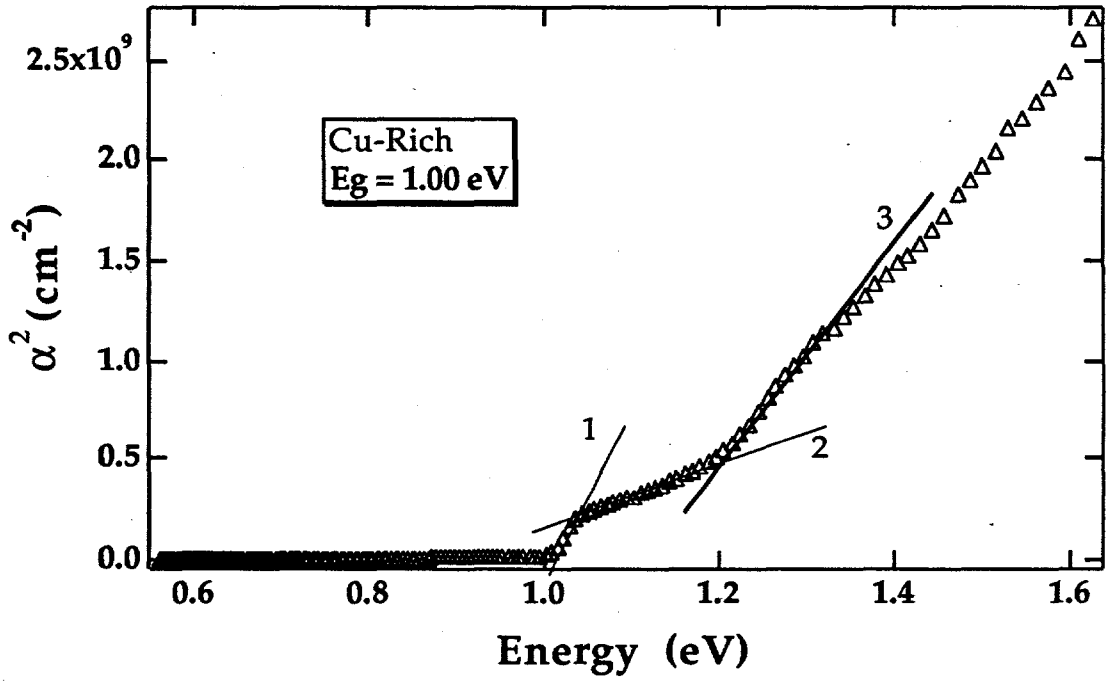

Figure 38. *Plot of α^2 Versus Incident Photon Energy for a Co-Deposited, Cu-Rich Sample Processed Under the Conditions of Corner 8. The Transitions are Numbered for Reference.*

determined by extrapolating the linear portion of the α^2 curve to the photon energy axis intercept. The primary transitions (transition 1) for all samples were around 1.0 eV. Transition number two in the Cu-rich and stoichiometric samples is of unknown origin at this time. Because it appears only in samples with significant quantities of $Cu_{2-x}Se$, it is believed to be attributable to this binary in some way. Transition number three in the stoichiometric and Cu-rich films, and transition number two in the Cu-poor film evident in the α^2 plots is the spin-orbit valence band splitting of ~0.22 eV. A comparison of the Cu-rich and Cu-poor data is shown in Figure 39. It should be noted that the optical data for films grown by RTP also agrees with published data [21] for single

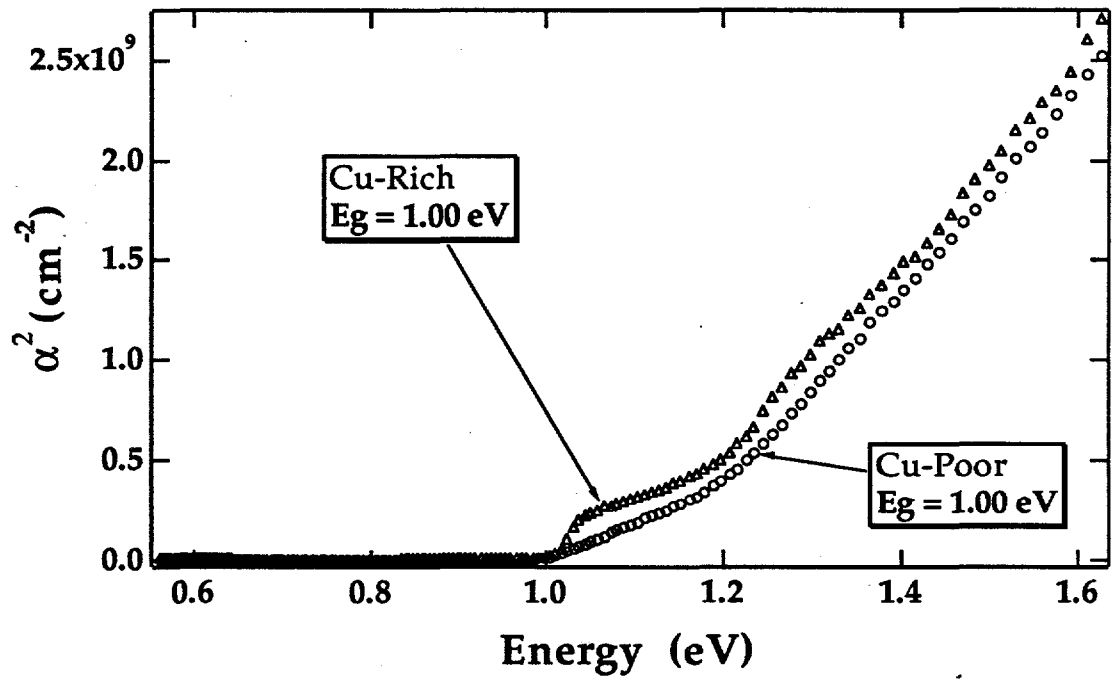

Figure 39. ***Plot of α^2 Versus Incident Photon Energy Comparing the Transitions of Cu-Poor and Cu-Rich Films.***

layered films vacuum deposited and reacted *in-situ* by elevated substrate temperatures.

As previously refered to, the slope of the linear portion of the first

transition can be used to calculate the effective masses of the electrons or holes. Solving for m^*_h in equation E-8, using A* values determined from linear fits to the α^2 plots in all three composition regions, and using a value of $.09m_e$ reported in the literature [22] for the effective mass of the electrons, we are able to calculate the effective mass for the holes in the upper valence band. The results are shown in Table V.

Table V. ***Values for A* and Subsequent Hole Effective Masses***

Composition Region	A*	m^*_h/m_e
Cu-Poor	1.881×10^9	.126
Stoichiometric	8.693×10^9	.100
Cu-Rich	5.476×10^9	.096

These values are of the same order as others published, but caution should be used before taking the values as absolutes because there are disagreements in some quarters over values of 2π in the expression for A*.

2.2 iv Scanning Electron Microscopy of CIS Thin Films Formed by RTP.

Scanning Electron Micrographs (SEM) of films processed at the conditions of Figure 17 show that significant recrystallization occurred during annealing as evidenced from increased grain size. Figure 40 shows SEM photographs of stoichiometric CIS films processed under the conditions of corner six of Figure 17 and its precursor. As is seen in the figure, the grain size was increased by the

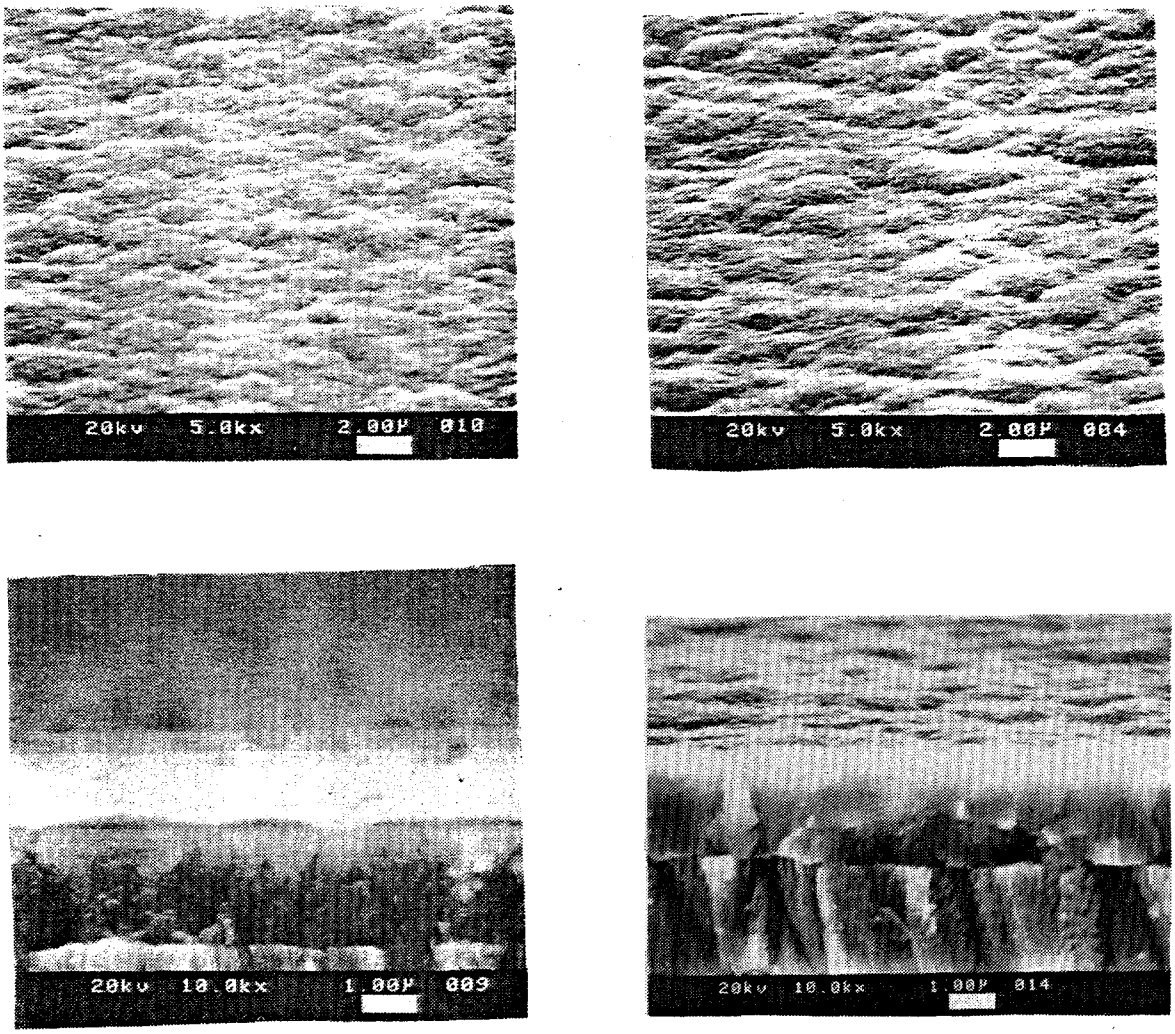

(a) (b)

Figure 40. *Scanning Electron Micrographs of (a) Stoichiometric Precursor and (b) the Same Film Processed Under the Conditions of Corner 6. The Upper Layer in the Edge Views is CIS, the Lower is Mo.*

RTP while the surface morphology remained relatively smooth. SEMs are also shown in Figures 41 and 42 for Cu-poor and Cu-rich samples processed under the same conditions as the stoichiometric sample of Figure 40. Significant recrystallization was also observed for these films with the surface morphology

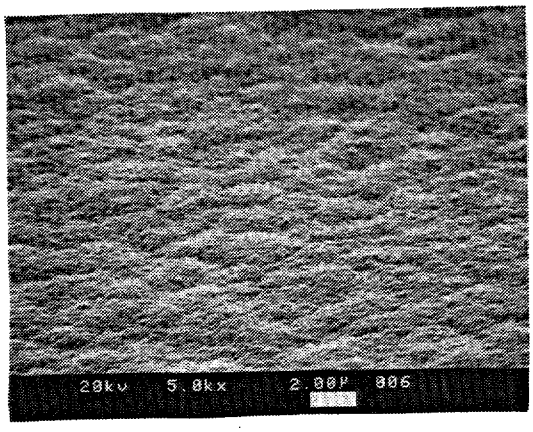

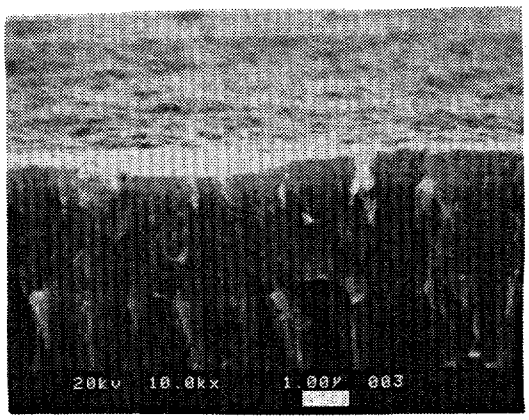

Figure 41. *Scanning Electron Micrographs of a Cu-Poor Film Processed at the Conditions of Corner 7.*

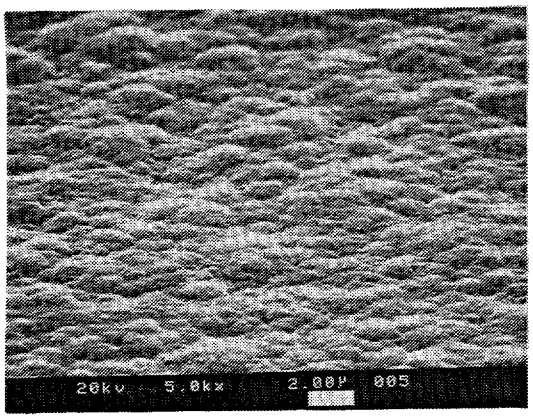

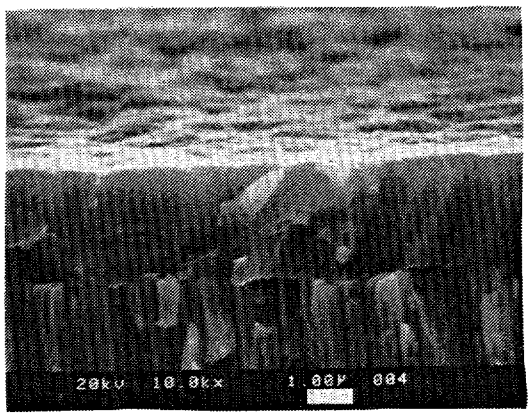

Figure 42. *Scanning Electron Micrographs of a Cu-Rich Film Processed Under the Conditions of Corner 8.*

remaining relatively smooth during the anneal. The very large grains evident in the Cu-rich sample are indicative of the $Cu_{2-x}Se$ incorporation in the film. SEMs have been made for all samples processed at the conditions of the experimental matrix in all three composition regions. Very little difference was observed, however, from the samples in the above figures.

2.2 v Large Single Crystal CIS Formation by the Rapid Thermal Processing of Unreacted Co-Deposited Thin Films.

During the preliminary experiments discussed at the beginning of this chapter, processes were attempted to determine the annealing temperature limits. While processes using final anneal temperatures under 800 °C produced films with large volume recrystallization and morphologies amenable to device fabrication, the anneals at 800 °C produced very large (> 20 μm), faceted single crystalline CIS. Figure 43 shows one of these films from several different perspectives. The film that was processed was of the structure Al_2O_3/Mo/Cu+In+Se with the Cu+In+Se layer being ~2.5 μm. The anneal profile consisted of a 10 °C/s ramp-up rate, a final anneal time of 30 seconds, and a final anneal temperature of 800 °C.

As is seen in the SEMs, the growth of the single crystals was detrimental to the overall surface morphology of the film. It appears as though the growth of the crystals was vertical, taking in surrounding material. This is evident from the edge view in Figure 41. The crystal shown there is > 4μm thick although the precursor was only 2.5 μm thick. This film was a section of the precursor shown in Figure 40. Evidence of the single crystalline nature of the material comes from X-ray diffraction analysis and EPMA. The XRD pattern of this film is shown in Figure 44. The intensity of the (112) reflection for the sample annealed at 800 °C increased five times because of enhanced crystal growth and preferred orientation effects.

Selective EPMA also verified the existence of the single crystal. The composition of the crystallites was 24.62/24.69/49.37/1.32 (at. percent Cu/In/Se/O) while the material between the crystallites had a composition of 20.92/25.34/47.70/6.05. These data are consistent with the XRD data; the

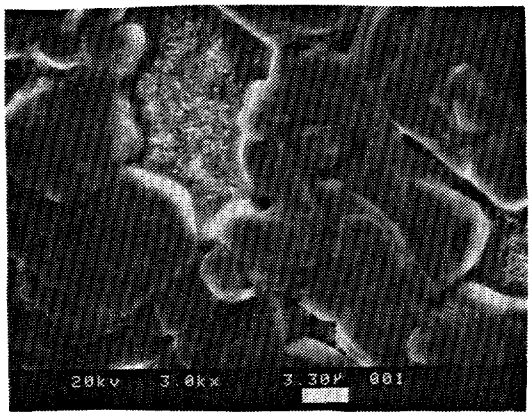

(a)

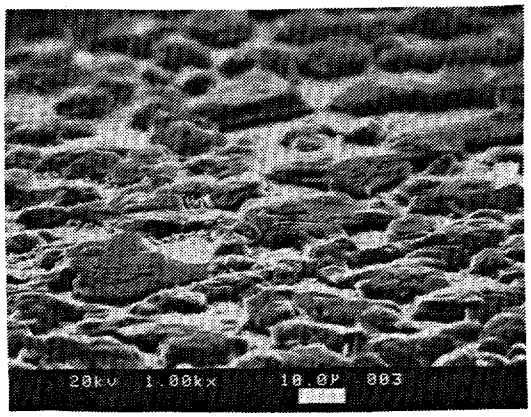

(b)

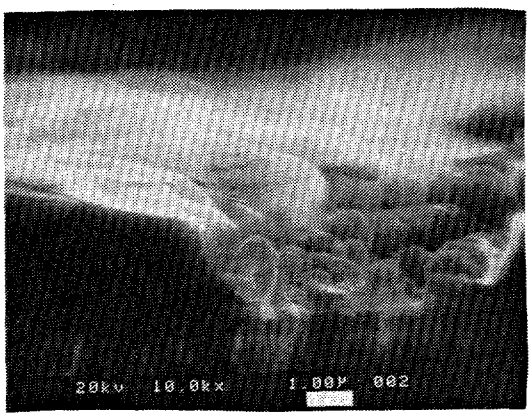

(c)

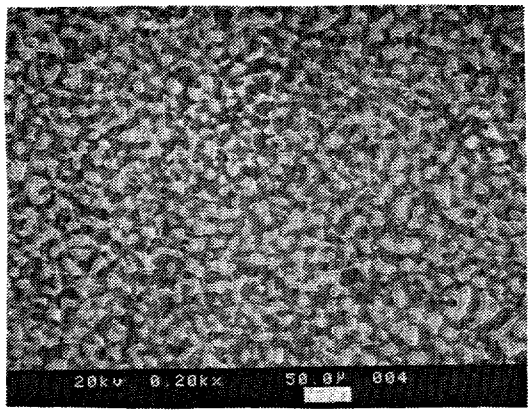

(d)

Figure 43. ***Scanning Electron Micrographs of Large Grain CIS. (a) View Showing 10-20 µm Faceted Single Crystals. (b) Angled View of Substrate Surface. (c) Edge View Showing 4 µm Thick Crystal and Material in Between Crystals. (d) Wide Angle View Showing Degree of Crystal Coverage. The Dark Areas are the Crystals.***

crystallites were responsible for the CIS peaks, while the material between is composed of In-Se, Cu-Se, and In-O binaries.

The mechanisms by which these crystals have grown are unknown at

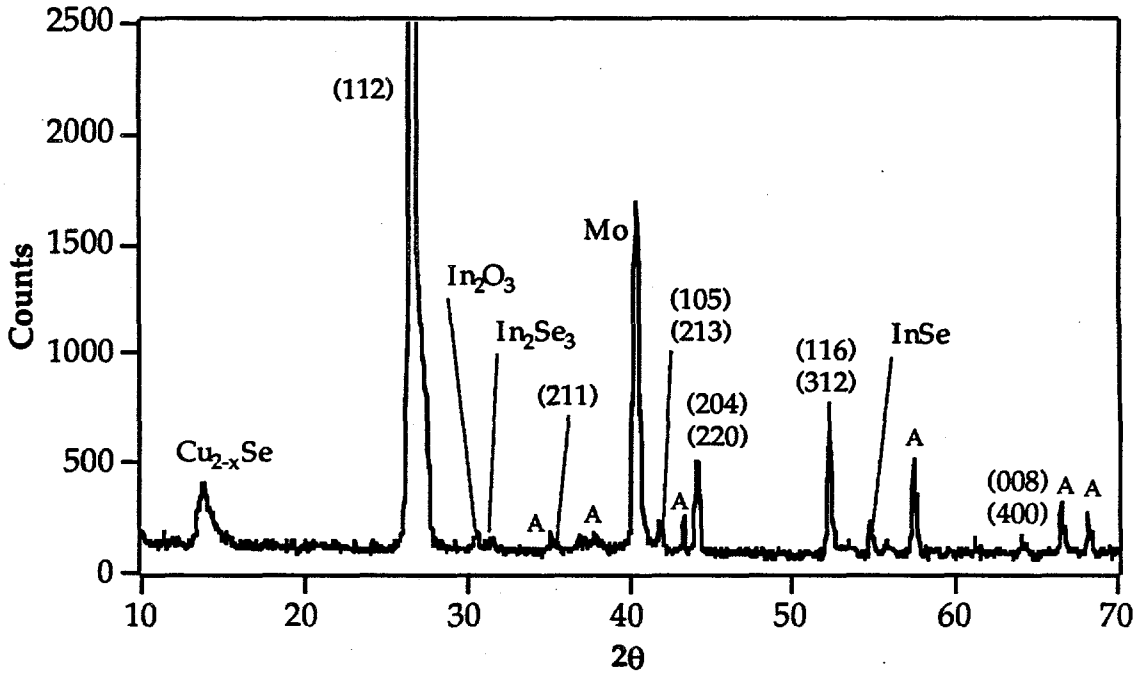

Figure 44. *XRD Data of Sample With 20 μm Single Crystals. Binaries are Indicative of the Material Between the Crystals.*

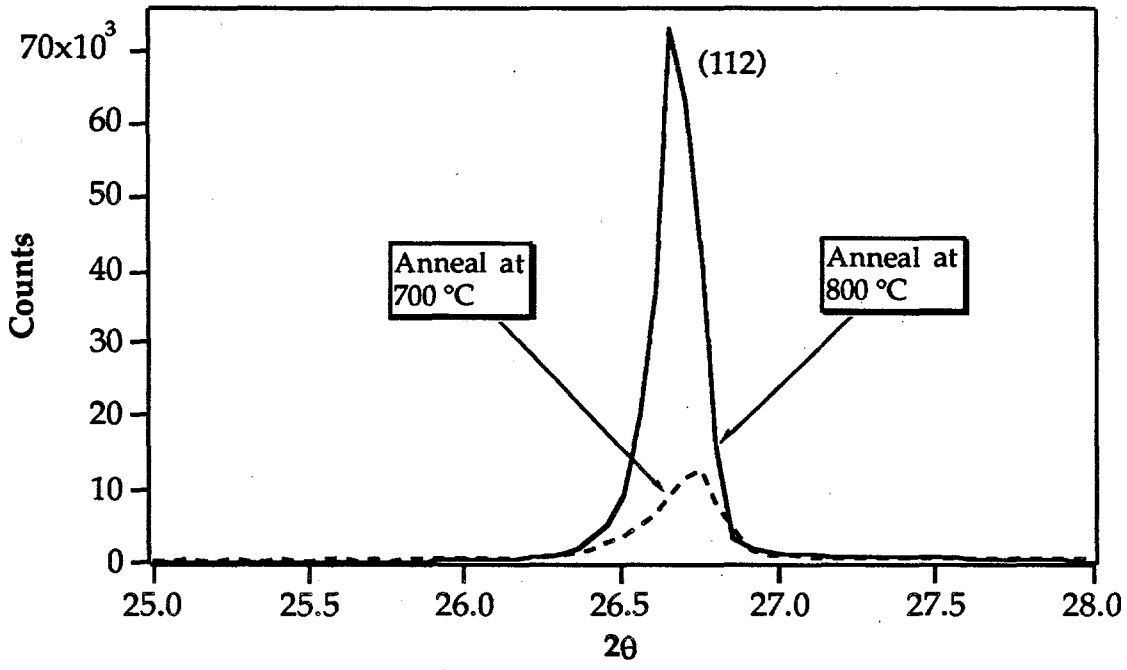

Figure 45. *(112) Peaks Comparison of the Sample Shown in Figure 26 and the Sample with 20 μm Single Crystals.*

present. One possible explanation comes from a close look at the pseudobinary phase diagram of Figure 3-12 of Ref. 23. For stoichiometric material (50% Cu_2Se/50% In_2Se_3), the melting point is shown to be at about 986 °C, so a melting and subsequent recrystallization of single phase CIS can be ruled out. However, at the position of the stoichiometric line of the phase diagram, there are several interesting phases that could affect the impurity phases found in our stoichiometric and Cu-rich film. At a temperature of 790 °C, for example, there is a eutectic at 89 mole percent Cu_2Se. One possible scenerio, then, is that these binary impurities melt, providing liquid phases for enhanced atom transport and reaction or perhaps providing nucleation sites for enhanced crystal growth. This work has been explored in more detail by colleagues at SERI with single crystals >100 μm grown [24]. We look forward to further study in this area with a goal of large grain growth with continuous substrate coverage.

3.0 CIS/CdS Device Fabrication Using CIS Formed by Rapid Thermal Processing.

We have conducted preliminary experiments to prove the material made by the rapid thermal process was indeed device quality. As stated earlier, the best devices have been made by using a multi-compositional approach to the fabrication of CIS in devices. The approach uses Cu-rich material at the Mo interface (for ohmic contact) and Cu-poor material at the CIS/CdS interface (to inhibit Cu diffusion into the CdS, which degrades the junction).

We have attempted to make devices using three different structures. The first was to make a device using single layered stoichiometric CIS with a subsequent layer of CdS. This device showed some photovoltaic effect, however,

as expected, the properties were poor, with very low V_{oc} and I_{sc}. We also used a bilayer approach with a structure of Al_2O_3/Mo/2.5 μm Cu-rich/.8 μm Cu-poor/CdS. This device was slightly better than the single layer device structure, but efficiencies were still only in the one percent range. A trilayer approach yielded our best (but still modest) results, producing devices of slightly over three percent. This structure is shown in Figure 46 with the device's I-V curve and its properties shown in Figure 47. The CIS for the device of Figure 47

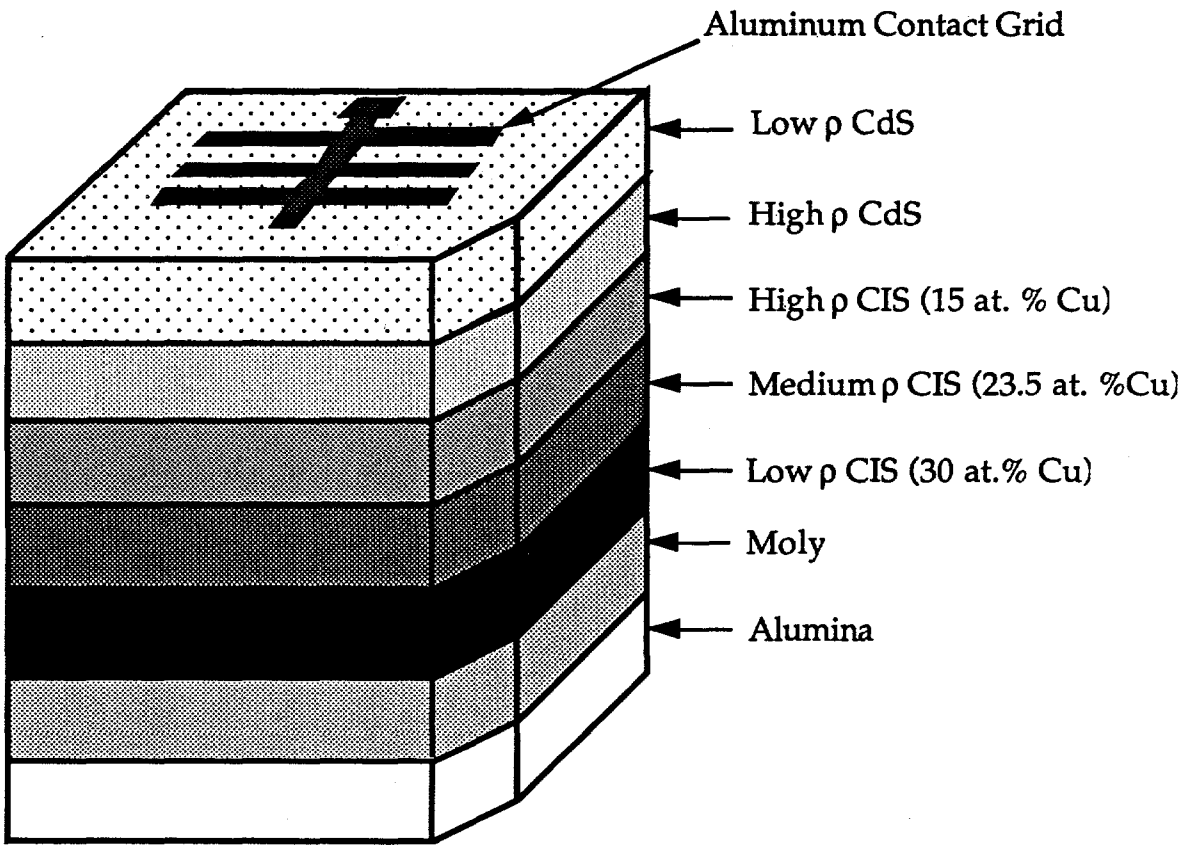

Figure 46. ***Tri-Layer Device Structure.***

was formed under the conditions of corner seven of the experimental matrix. A description of the entire device fabrication process is as follows: First, the CIS

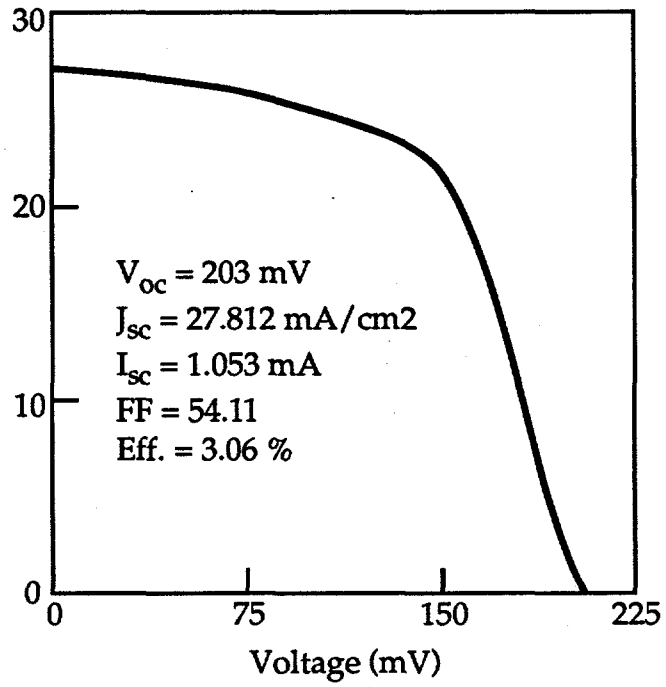

Figure 47. ***Device Results for Structure Shown in Figure 44. CIS Formed by RTP Under the Conditions of Corner 7 of the Experimental Matrix.***

was deposited by co-evaporation adjusting the Cu flux to form the tri-layer. The unreacted material was then recrystallized by RTP to form the CIS. The CdS was then deposited by thermal evaporation in two layers as shown. The resistivity of the CdS was controlled by In doping. Next, an aluminum contact grid was deposited by electron beam evaporation. The sample was then put through a photolithography process in order to etch away extraneous CdS and define an active area for the device. It should also be noted that CIS for these devices was fabricated at the range of conditions of the experimental matrix. We have shown the best results of all these samples. It should be noted that no correlation between the RTP conditions and device performance was immediately evident.

The purpose of our device work was to lend credence to the concept of the RTP. As is seen, the number of variables in the device fabrication process is

very large, and optimization of the process will be a significant, multiple-year project. The reason for our small device efficiency is the low V_{oc}. Assuming the CdS deposition and photolithography processes were optimized, this might indicate contamination at the interface, possibly by binaries or oxides. Chemical treatments will be attempted to determine if this is in fact the case. Our results do, however, give much promise to this technique for making device quality CIS with processing times of less than two minutes.

4.0 References

1. D. S. Albin, G. D. Mooney, J. Carapella, A. Duda, J. Tuttle, R. Matson, and R. Noufi, to be published in *Solar Cells*..

2. G. David Mooney, *Rapid Recrystallization of Semiconductor Thin Films for Photovoltaic Applications*, Ph.D. Dissertation, 1990, p. 165.

3. G. David Mooney, *Rapid Recrystallization of Semiconductor Thin Films for Photovoltaic Applications*, Ph.D. Dissertation, 1990, p. 77.

4. G. David Mooney, *Rapid Recrystallization of Semiconductor Thin Films for Photovoltaic Applications*, Ph.D. Dissertation, 1990, p. 79.

5. Rommel Noufi and John Dick, *J. Appl. Phys.*, **58**, 3884 (1985).

6. G. David Mooney, *Rapid Recrystallization of Semiconductor Thin Films for Photovoltaic Applications*, Ph.D. Dissertation, 1990, p. 66.

7. G. David Mooney, *Rapid Recrystallization of Semiconductor Thin Films for Photovoltaic Applications*, Ph.D. Dissertation, 1990, p. 47.

8. John R. Tuttle, *An Optical and Microstructural Characterization Study and Microstructural Model of Co-Evaporated Polycrystalline Thin Film $CuInSe_2$ For Photovoltaic Applications*, Ph.D. Dissertation, 1990, p. 141.

9. G. David Mooney, *Rapid Recrystallization of Semiconductor Thin Films for Photovoltaic Applications*, Ph.D. Dissertation, 1990, p. 171.

10. Jacques I. Pankove, *Optical Processes in Semiconductors*, (Dover Publications, New York, 1971).

11. Frederick Wooten, *Optical Properties of Solids*, (Academic Press, San Diego, 1972).

12. G. David Mooney, *Rapid Recrystallization of Semiconductor Thin Films for Photovoltaic Applications*, Ph.D. Dissertation, 1990, p. 52.

13. G. David Mooney, *Rapid Recrystallization of Semiconductor Thin Films for Photovoltaic Applications*, Ph.D. Dissertation, 1990, p. 10.

14. G. David Mooney, *Rapid Recrystallization of Semiconductor Thin Films for Photovoltaic Applications*, Ph.D. Dissertation, 1990, p. 12.

15. J. Bardeen, F. J. Blatt, and L. H. Hall, *Proc. of Atlantic City Photoconductivity Conference*, (J. Wiley and Chapman and Hall, 1956), p. 146.

16. Jacques I. Pankove, *Optical Processes in Semiconductors*, (Dover Publications, New York, 1971), p. 94.

17. R. E. Denton, R. D. Campbell, and S. G. Tomlin, J. Phys., **D5**, 852 (1972).

18. John R. Tuttle, *An Optical and Microstructural Characterization Study and Microstructural Model of Co-Evaporated Polycrystalline Thin Film $CuInSe_2$ For Photovoltaic Applications*, Ph.D. Dissertation, 1990, p. 115.

19. G. David Mooney, *Rapid Recrystallization of Semiconductor Thin Films for Photovoltaic Applications*, Ph.D. Dissertation, 1990, p. 187.

20. John R. Tuttle, *An Optical and Microstructural Characterization Study and Microstructural Model of Co-Evaporated Polycrystalline Thin Film $CuInSe_2$ For Photovoltaic Applications*, Ph.D. Dissertation, 1990, p. 121.

21. J. R. Tuttle, D. Albin, R. J. Matson, and R. Noufi, *J. Appl. Phys.*, **66**, 4408(1989).

22. Taizo Irie, Saburo Endo, and Shiegeo Kimura, Jpn. J. Appl. Phys., **18**, 1303 (1097).

23. G. David Mooney, *Rapid Recrystallization of Semiconductor Thin Films for Photovoltaic Applications*, Ph.D. Dissertation, 1990, p. 63.

24. D. S. Albin, G. D. Mooney, A. Duda, J. Tuttle, R. Matson, and R. Noufi, to be published in *Solar Cells*..

5.0 Abstract

Photovoltaics promise to be an important source of energy for the future. Unlike fossil fuels, this resource is clean and virtually unlimited. Although the technology is developed, photovoltaics are not used widely because the costs are not yet competitive with fossil fuels.

One of the most promising materials for use in photovoltaic devices is thin film polycrystalline $CuInSe_2$. This material holds the current energy conversion efficiency record for a polycrystalline thin film material. The techniques used to produce these devices, however, have features undesirable for mass production such as highly toxic gases and lengthy thermal anneals. The goal of this work was to explore new, safe methods of fabricating device quality $CuInSe_2$. Fundamental characterization techniques showed the properties of the co-deposited films subjected to Rapid Thermal Processing (RTP) to be comparable, and in some cases superior, to films grown by more conventional methods. Characterization included structural and phase studies by X-ray diffraction analysis, investigation of optical properties and electronic band structures by reflection and transmission spectroscopy, studies of composition and modeling the dynamics of film growth during the process by electron probe for microanalysis, and the effects of the process on grain growth and morphology by scanning electron microscopy.

Rapid thermal processing of vacuum co-deposited Cu, In, and Se subjects films to a heating by radiation using tungsten quartz lamps. Using this method, we successfully fabricated photovoltaic device quality $CuInSe_2$ using post-deposition processing times of less than two minutes. All processing was carried out in an inert argon atmosphere. Films processed by this method were nearly single phase $CuInSe_2$ with the expected chalcopyrite structure (tetragonal symmetry) and the expected lattice parameters. The optical spectroscopy showed a distinct, direct valence to conduction band transition of 1.0 eV and a spin-orbit transition of 0.22 eV. Absorption coefficients have been in the 5×10^4 cm^{-1} range. We also successfully targeted various compositions while identifying intermediate phases formed and their subsequent evaporation and/or incorporation into the film. These films had enhanced grain growth with morphologies suitable for device fabrication. Preliminary device characteristics with appropriate theoretical modeling are also presented.

Acknowledgments

The authors gratefully acknowledge the contributions to this work of Rommel Noufi, John Tuttle, Dave Albin, Rick Mitchell and Ken Zweibel of the Solar Energy Research Institute. Their involvement in the project was invaluable.

Document Control Page	1. SERI Report No. NREL/TP-411-4752	2. NTIS Accession No. DE92001222	3. Recipient's Accession No.

4. Title and Subtitle

Novel Thin-Film $CuInSe_2$ Fabrication

5. Publication Date

February 1992

6.

7. Author(s)

G.D. Mooney and A.M. Hermann

8. Performing Organization Rept. No.

9. Performing Organization Name and Address

University of Colorado
Department of Physics
Boulder, CO 80309-0390

10. Project/Task/Work Unit No.

PV231101

11. Contract (C) or Grant (G) No.

(C) XC-0-10012-1

(G)

12. Sponsoring Organization Name and Address

National Renewable Energy Laboratory
1617 Cole Blvd.
Golden, CO 80401-3393

13. Type of Report & Period Covered

Technical Report
1 March 1990 - 30 April 1991

14.

15. Supplementary Notes

NREL technical monitor: R. Mitchell

16. Abstract (Limit: 200 words)

This report describes research in Rapid Thermal Processing (RTP), a process that allows the formation of $CuInSe_2$ without the use of H_2Se. RTP is a well-established method of rapidly achieving temperatures necessary to melt and recrystallize materials such as Si and silicides. RTP processes can rapidly and uniformly heat large surface areas to hundreds of degrees Celsius. RTP is the most promising method of rapid recrystallization studied to date, being readily scalable from the research to the production level. The approach to the experiment was divided into two sections: (1) fabricating the precursor film and (2) processing the precursor film. The objective of the first phase of the work was to fabricate the thin films by RTP, then fully characterize them, to demonstrate the viability of the process as a method by which to make device-quality $CuInSe_2$. The second phase was to demonstrate that material made by this method could be used to make an active photovoltaic device.

17. Document Analysis

a. Descriptors

thin films ; $CuInSe_2$; photovoltaics ; solar cells ; fabrication ; processing

b. Identifiers/Open-Ended Terms

c. UC Categories

273

18. Availability Statement

National Technical Information Service
U.S. Department of Commerce
5285 Port Royal Road
Springfield, VA 22161

19. No. of Pages

69

20. Price

A04

Form No. 0069E (6-30-87)